Non-Hermitian Michelson interferometer for exceptional-point-enhanced sensing

Zhihao Xie [1,*] Jianghua Cheng [2,*] Yuwei Jing,[1] Yahui Cai [2] Jiangshan Tang,[1,3] Tao Li [4,5,†] and Keyu Xia [1,6,7,‡]

[1]*College of Engineering and Applied Sciences, National Laboratory of Solid State Microstructures, Nanjing University, Nanjing 210023, China*

[2]*College of Electronic Science and Technology, National University of Defense Technology, Changsha 410073, China*

[3]*College of Advanced Interdisciplinary Studies, National University of Defense Technology, Changsha 410073, China*

[4]*MIIT Key Laboratory of Semiconductor Microstructure and Quantum Sensing, School of Physics, Nanjing University of Science and Technology, Nanjing 210094, China*

[5]*Engineering Research Center of Semiconductor Device Optoelectronic Hybrid Integration in Jiangsu Province, Nanjing 210094, China*

[6]*Hefei National Laboratory, Hefei 230088, China*

[7]*Jiangsu Key Laboratory of Quantum Information Science and Technology, Nanjing University, Suzhou 215163, China*

(Received 31 October 2025; accepted 25 September 2026; published 14 October 2026)

The Michelson interferometer underpins modern optical metrology, enabling precise measurements of displacement and gravitational waves. However, the sensitivity of the conventional Hermitian Michelson interferometer is inherently limited by its linear response to a perturbation. Here, we propose a non-Hermitian Michelson interferometer by introducing a coupling between two arms with reservoir engineering, forming a configuration of light cross. The eigenfrequency splitting as a spectral response displays a square-root dependence on a perturbation. Remarkably, the quantum Fisher information of our non-Hermitian Michelson interferometer can exceed that of its Hermitian counterpart by more than three orders when Brownian noise is included, implying a great enhancement in sensitivity. This work provides a framework for non-Hermitian interferometric sensing with unprecedented sensitivity.

DOI: 10.1103/ssrq-2fb2

I. INTRODUCTION

The Michelson interferometer (MI) has been a pivotal tool in optical metrology for both historical validation of the constancy of the speed of light [1] and modern applications ranging from displacement sensing to gravitational-wave detection [2–7]. Its operation relies on converting phase variations or changes of arm lengths into intensity modulations, enabling precise measurements of displacement [8,9], refractive index [10,11], and temperature [12,13]. In landmark applications such as LIGO, kilometer-scale MIs have achieved high sensitivity for detecting spacetime fluctuations [2–7]. Essentially, the kilometer-long arms in LIGO are used to amplify the very weak signal. However, a fundamental limitation of conventional MIs arises from their intrinsic linear response [14–16]: the signal-induced phase shift or perturbation of the arm length is mapped linearly into a change of output intensity. While this linear response simplifies signal retrieval, it imposes a trade-off between measurement sensitivity and physical constraints such as arm length and quantum noise [17–20]. Significant efforts, including the use of quantum squeezed light, have been made to suppress quantum noise and enhance sensitivity [7,21–24]. Nevertheless, improving the response and sensitivity of MIs in the weak-signal regime is highly desired but remains a formidable challenge.

Brownian noise, also referred to as thermal noise, is inevitable in many realistic applications [25–27], particularly in optomechanical sensors. In precision measurements, thermal noise imposes a fundamental constraint in sensitivity [28,29]. It originates from the coupling of the system to its surrounding thermal environment, leading to stochastic fluctuations that cannot be eliminated. In state-of-the-art interferometers, such as gravitational-wave detectors, suppressing thermal noise has been a central challenge [30–32]. For instance, intensive efforts in LIGO have been devoted to reducing Brownian noise via advanced mirror-coating technologies [33,34], thereby substantially improving the signal-to-noise ratio in precision measurements. Similarly, in atomic interferometry and related precision measurement platforms, significant progress has been made by mitigating thermal noise, leading to enhanced performance in atomic clocks [35,36], nuclear clocks [37], and gravimeters [38,39]. Thus, it can suppress Brownian noise in interferometric sensing schemes.

Non-Hermitian physics has witnessed rapid advances, ranging from non-Hermitian topology [40–53], the skin effect [54,55], and chiral transport [56,57] to non-Hermitian lasing [58], emerging directions in sensing [50,59–72]. In the context of sensing, despite serious debates regarding the capability of gain-loss platforms to achieve genuine sensitivity enhancement [73–76], recent progress in non-Hermitian sensing operating near an exceptional point (EP), where both eigenvalues and eigenvectors coalesce, has demonstrated a sublinear spectral response to circumvent the limitation of linear-scaling response in Hermitian sensors [50,60–72,77–87] and promises dramatic

*These authors contributed equally to this work.
†Contact author: tao.li@njust.edu.cn
‡Contact author: keyu.xia@nju.edu.cn

 ©2026 American Physical Society

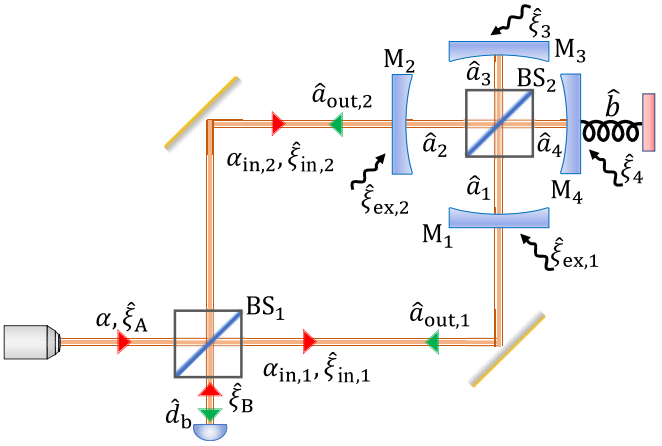


FIG. 1. Schematic of the NHMI. A coherent probe field is input into the NHMI from the left side. It is divided by the beam splitter BS_1 into two parts, driving the cavity modes $\hat{a}_1$ and $\hat{a}_2$ via the mirrors M_1 and M_2, respectively. The arm cavities are mixed by the beam splitter BS_2 and decay into the common reservoirs through the mirrors M_3 and M_4 with different rates. $\hat{\xi}_{ex,1}$, $\hat{\xi}_{ex,2}$, $\hat{\xi}_3$, and $\hat{\xi}_4$ denote quantum noises entering the system via the mirrors. $\hat{\xi}_{in,1}$ and $\hat{\xi}_{in,2}$ denote quantum noises entering the system via the beam splitter. The vibration mode $\hat{b}$, subject to thermal noise, couples to $\hat{a}_4$ via the mirror M_4.

sensitivity enhancement. The non-Hermiticity-enhanced sensitivity has been observed in various resonator-based platforms [63–65,88]. Despite many advances, the incorporation of EP-enhanced response and sensitivity into MIs is yet to be explored.

In this paper, we fill this gap by proposing a *passive* and *linear* non-Hermitian MI (NHMI) with a light-cross configuration. In this configuration, the two arms are dissipatively coupled with reservoir engineering [89,90], forming an anti-parity-time (APT) symmetric MI. This NHMI displays a square-root eigenfrequency splitting as a response to perturbations of arm length change and thus suppresses the fundamental Brownian noise. Consequently, the scheme achieves superior metrological performance compared to its Hermitian counterpart (HMI).

The remainder of this paper is organized as follows. In Sec. II, we introduce the theoretical model of the NHMI and derive its transmission spectrum. In Sec. III, we investigate the sensing performance of the NHMI. Finally, Sec. IV summarizes our main findings and discusses their implications. Detailed derivations of the Hamiltonians, output spectra, and the quantum Fisher information (QFI) for the NHMI and HMI are presented in Appendixes A, B, and C, respectively.

II. SYSTEM AND MODEL

The system is schematically shown in Fig. 1. A MI consists of two optical arms, each including a Fabry-Pérot cavity, supporting modes $\hat{a}_1$ and $\hat{a}_2$. The two cavities are situated at the ends of each arm to enhance light-signal interaction. The beam splitter BS_1 divides the probe laser field into two paths and feeds them into the two arms. This BS_1 also combines the reflections off the two cavities $\hat{a}_1$ and $\hat{a}_2$ to generate an interference output $\hat{d}_b$. In a conventional HMI, the two cavities are decoupled and decay at the same rate [2–7,91]. In our light cross, the two cavity modes are mixed by the BS_2. This BS_2 converts modes $\hat{a}_1$ and $\hat{a}_2$ into the auxiliary supermodes [92] via $\hat{a}_3 = \cos\theta'\hat{a}_1 - ie^{-i\varphi'}\sin\theta'\hat{a}_2$ and $\hat{a}_4 = \cos\theta'\hat{a}_2 - ie^{i\varphi'}\sin\theta'\hat{a}_1$, where $\cos\theta'$ and $\sin\theta'$ are reflection and transmission amplitudes of the BS_2, respectively, and φ' is the relative phase between the two transmitted modes. These two supermodes decay via the cavity mirrors M_3 and M_4 with rates $\kappa_{ex,3}$ and $\kappa_{ex,4}$, respectively. Throughout the investigation below, we set $\theta' = \pi/4$ and $\varphi' = \pi/2$.

The cavity modes $\hat{a}_1$ and $\hat{a}_2$ share two common reservoirs via the supermodes. This reservoir-sharing decay can build up a dissipative coupling between modes $\hat{a}_1$ and $\hat{a}_2$ with *reservoir engineering* [89,90]. Specifically, by introducing differential mirror-induced losses, i.e., $\kappa_{ex,3} \neq \kappa_{ex,4}$, we create an anti-parity-time symmetric coupling between $\hat{a}_1$ and $\hat{a}_2$ (see Appendix A). This configuration realizes a NHMI with an interaction Hamiltonian:

$$H_{APT} = -ig(\hat{a}_1^\dagger\hat{a}_2 + \hat{a}_2^\dagger\hat{a}_1), \tag{1}$$

where $g = (\kappa_{ex,4} - \kappa_{ex,3})/4$. This is the key point of this work. When $g = 0$, this system reduces to a HMI. The losses of cavity mirrors M_3 and M_4 also introduce an additional decay rate $(\kappa_{ex,3} + \kappa_{ex,4})/4$ to both modes $\hat{a}_1$ and $\hat{a}_2$.

In this system, the arm lengths of modes $\hat{a}_3$ and $\hat{a}_4$ are equal, much smaller than those of modes $\hat{a}_1$ and $\hat{a}_2$. In the absence of perturbation, modes $\hat{a}_1$ and $\hat{a}_2$ are assumed to have the same arm length L and resonance frequency ω_0. A perturbation like a gravitational wave or an effective displacement respectively causes an opposite displacement of arm length $\delta L/2$ to modes $\hat{a}_1$ and $\hat{a}_2$, effectively yielding a shift, $\delta_s = \omega_0\delta L/2L$, to their resonance frequencies. The probe fields drive modes $\hat{a}_1$ and $\hat{a}_2$ via the mirrors M_1 and M_2 at the external decay strengths $\kappa_{ex,1}$ and $\kappa_{ex,2}$, respectively. We neglect the intrinsic losses of the cavities but only consider losses introduced by the cavity mirrors. Modes $\hat{a}_1$ and $\hat{a}_2$ respectively decay at rates $\kappa_1 = \kappa_{ex,1}/2 + (\kappa_{ex,3} + \kappa_{ex,4})/4$ and $\kappa_2 = \kappa_{ex,2}/2 + (\kappa_{ex,3} + \kappa_{ex,4})/4$ (see Appendix A). For simplicity, we set $\kappa_{ex,1} = \kappa_{ex,2} = \kappa_{ex}$, yielding $\kappa_1 = \kappa_2$. We denote $\kappa = \kappa_1 = \kappa_2$. Essentially, this light cross is an APT-symmetric NHMI. It can operate near an EP, enhancing sensitivity via the square-root dependence on perturbation. In a frame rotating at the frequency ω_p, the effective free Hamiltonian is given by

$$H_0 = (\Delta + \delta_s - i\kappa)\hat{a}_1^\dagger\hat{a}_1 + (\Delta - \delta_s - i\kappa)\hat{a}_2^\dagger\hat{a}_2, \tag{2}$$

with the detuning $\Delta = \omega_0 - \omega_p$. The dynamics of the NHMI is governed by the APT-symmetric Hamiltonian $H_s = H_{APT} + H_0$. We measure the perturbation by determining the eigenfrequency splitting of the system. Notably, we create an APT-symmetric NHMI without introducing a gain, avoiding the gain-induced noise.

Obviously, the eigenvalues of the MI are given by

$$\lambda_\pm = \Delta - i\kappa \pm \sqrt{\delta_s^2 - g^2}. \tag{3}$$

The real eigenfrequencies split by an amount of

$$\Delta\lambda = \mathrm{Re}[\lambda_+] - \mathrm{Re}[\lambda_-] = 2\sqrt{\delta_s^2 - g^2}. \tag{4}$$

For $g = 0$, the system is a HMI and this splitting displays a linear-scaling response, $\Delta\lambda = 2\delta_s$. While for $g \neq 0$, the system becomes a NHMI and exhibits a square-root response to perturbation when the signal δ_s is biased near EP $\delta_{EP} = |g|$.

We retrieve the eigenvalues by fitting the output spectrum. A coherent probe laser field with mean amplitude α and frequency ω_p is injected into the MI through the BS_1. The output spectrum is obtained by sweeping the frequency of the probe field. After BS_1, the total field is the sum of the probe field and quantum noise. The coherent amplitudes driving the cavity modes $\hat{a}_1$ and $\hat{a}_2$ are related to the input amplitude α by $\alpha_{in,1} = \cos\theta\,\alpha$ and $\alpha_{in,2} = -ie^{-i\varphi}\sin\theta\,\alpha$, respectively, where θ and φ are defined as for BS_2. We set $\varphi = \pi/2$. The driving Hamiltonian is given by

$$H_{dr} = i\sqrt{\kappa_{ex}}(\alpha^*_{in,1}\hat{a}_1 - \hat{a}_1^\dagger\alpha_{in,1}) + i\sqrt{\kappa_{ex}}(\alpha^*_{in,2}\hat{a}_2 - \hat{a}_2^\dagger\alpha_{in,2}). \tag{5}$$

Quantum vacuum noise inevitably enters the system via the BS and the cavity mirrors, and subsequently limits the measurement sensitivity. We denote the quantum noise modes entering the MI via the BS_1 by operators $\hat{\xi}_A$ and $\hat{\xi}_B$. They connect to the BS output fields via the relations $\hat{\xi}_{in,1} = \cos\theta\,\hat{\xi}_A - ie^{i\varphi}\sin\theta\,\hat{\xi}_B$ and $\hat{\xi}_{in,2} = -ie^{-i\varphi}\sin\theta\,\hat{\xi}_A + \cos\theta\,\hat{\xi}_B$. $\hat{\xi}_{ex,1}$ and $\hat{\xi}_{ex,2}$ denote quantum noises directly coupling to the cavity modes via mirrors M_1 and M_2 [93]. Then, the total quantum noises entering the cavity modes $\hat{a}_1$ and $\hat{a}_2$ via mirrors M_1 and M_2 are given by $\hat{\xi}_1 = \hat{\xi}_{in,1} + \hat{\xi}_{ex,1}$ and $\hat{\xi}_2 = \hat{\xi}_{in,2} + \hat{\xi}_{ex,2}$, respectively. Note that the value of φ is important for achieving sensitivity enhancement as discussed afterward. The operators $\hat{\xi}_3$ and $\hat{\xi}_4$ represent quantum noises coupling into cavity modes $\hat{a}_3$ and $\hat{a}_4$ via mirrors M_3 and M_4, respectively. The effect of the vacuum noises on the system can be described by the Hamiltonian (see Appendix A)

$$\begin{aligned}\hat{H}_{QV} = {} & i\sqrt{\kappa_{ex,3}/2}(\hat{\xi}_3^\dagger\hat{a}_1 - \hat{a}_1^\dagger\hat{\xi}_3) + i\sqrt{\kappa_{ex,4}/2}(\hat{\xi}_4^\dagger\hat{a}_2 - \hat{a}_2^\dagger\hat{\xi}_4) \\ & + i\sqrt{\kappa_{ex,4}/2}(\hat{\xi}_4^\dagger\hat{a}_1 - \hat{a}_1^\dagger\hat{\xi}_4) - i\sqrt{\kappa_{ex,3}/2}(\hat{\xi}_3^\dagger\hat{a}_2 - \hat{a}_2^\dagger\hat{\xi}_3) \\ & + i\sqrt{\kappa_{ex}}(\hat{\xi}_1^\dagger\hat{a}_1 - \hat{a}_1^\dagger\hat{\xi}_1) + i\sqrt{\kappa_{ex}}(\hat{\xi}_2^\dagger\hat{a}_2 - \hat{a}_2^\dagger\hat{\xi}_2). \end{aligned} \tag{6}$$

Importantly, Brownian noise is unavoidable in many realistic applications and can further decrease the sensitivity. To account for its effect, we incorporate thermal noise by introducing a mechanical mode $\hat{b}$ with frequency ω_b and damping rate γ_m. The mechanical mode couples to the supermode $\hat{a}_4$ via M_4 with strength g_{om}. It is driven by the environmental phonon operator $\hat{b}_{in}$ with $\langle\hat{b}_{in}\hat{b}_{in}^\dagger\rangle = n_{th} + 1$, where n_{th} is the thermal phonon number. The effect of Brownian noises can be described by the Hamiltonian (see Appendix A)

$$\begin{aligned}\hat{H}_{BN} = {} & \left(\omega_b - i\frac{\gamma_m}{2}\right)\hat{b}^\dagger\hat{b} + i\sqrt{\gamma_m}(\hat{b}_{in}^\dagger\hat{b} - \hat{b}^\dagger\hat{b}_{in}) \\ & + \frac{g_{om}}{2}(\hat{b}^\dagger + \hat{b})(\hat{a}_1^\dagger + \hat{a}_2^\dagger)(\hat{a}_1 + \hat{a}_2). \end{aligned} \tag{7}$$

Remarkably, the interaction between the supermode $\hat{a}_4$ and the mechanical mode $\hat{b}$ results in an effective three-mode coupling among $\hat{a}_1$, $\hat{a}_2$, and $\hat{b}$, which may induce intriguing physics to be explored.

The system evolution is governed by the Langevin equations:

$$\begin{aligned}\frac{d\hat{b}}{dt} = {} & \left(-i\omega_b - \frac{\gamma_m}{2}\right)\hat{b} - i\frac{g_{om}}{2}(\hat{a}_1^\dagger + \hat{a}_2^\dagger)(\hat{a}_1 + \hat{a}_2) - \sqrt{\gamma_m}\hat{b}_{in}, \\ \frac{d\hat{a}_1}{dt} = {} & [-i(\Delta' + \delta_s) - \kappa]\hat{a}_1 - g'\hat{a}_2 - \sqrt{\kappa_{ex}}(\alpha_{in,1} + \hat{\xi}_1) \\ & - \sqrt{\kappa_{ex,3}/2}\hat{\xi}_3 - \sqrt{\kappa_{ex,4}/2}\hat{\xi}_4, \\ \frac{d\hat{a}_2}{dt} = {} & [-i(\Delta' - \delta_s) - \kappa]\hat{a}_2 - g'\hat{a}_1 - \sqrt{\kappa_{ex}}(\alpha_{in,2} + \hat{\xi}_2) \\ & - \sqrt{\kappa_{ex,3}/2}\hat{\xi}_3 - \sqrt{\kappa_{ex,4}/2}\hat{\xi}_4, \end{aligned} \tag{8}$$

where $\Delta' = \Delta + g_{om}\langle\hat{b}^\dagger + \hat{b}\rangle/2$ and $g' = g + ig_{om}\langle\hat{b}^\dagger + \hat{b}\rangle/2$. In optomechanical systems, the radiation-pressure-induced frequency shift, $g_{om}\langle\hat{b}^\dagger + \hat{b}\rangle/2$, is negligible. Therefore, we approximate $\Delta' \simeq \Delta$ and $g' \simeq g$.

To obtain the steady-state output field $\hat{d}_b$, we linearize the cavity modes $\hat{a}_{1,2}$ and the mechanical mode $\hat{b}$ as $\hat{a}_{1,2} = \alpha_{1,2} + \delta\hat{a}_{1,2}$ and $\hat{b} = \alpha_b + \delta\hat{b}$, respectively. Here, $\alpha_{1,2} = \langle\hat{a}_{1,2}\rangle$ and $\alpha_b = \langle\hat{b}\rangle$ denote the mean amplitudes, given by

$$\begin{aligned}\alpha_1 = {} & \frac{\sqrt{\kappa_{ex}}[i(\Delta' - \delta_s) + \kappa]\alpha_{in,1} - \sqrt{\kappa_{ex}}g'\alpha_{in,2}}{-[i(\Delta' + \delta_s) + \kappa][i(\Delta' - \delta_s) + \kappa] + g'^2}, \\ \alpha_2 = {} & \frac{\sqrt{\kappa_{ex}}[i(\Delta' + \delta_s) + \kappa]\alpha_{in,2} - \sqrt{\kappa_{ex}}g'\alpha_{in,1}}{-[i(\Delta' + \delta_s) + \kappa][i(\Delta' - \delta_s) + \kappa] + g'^2}, \end{aligned} \tag{9}$$

where $\delta\hat{a}_1$, $\delta\hat{a}_2$, and $\delta\hat{b}$ represent the corresponding fluctuations. Using the input-output relations of optical cavities, the steady-state output field $\hat{d}_b$ is

$$\begin{aligned}\hat{d}_b = {} & F_0 + F_1\hat{\xi}_{ex,1} + F_2\hat{\xi}_{ex,2} + F_3\hat{\xi}_3 \\ & + F_4\hat{\xi}_4 + F_5\hat{\xi}_A + F_6\hat{\xi}_B + F_b\hat{b}_{in}, \end{aligned} \tag{10}$$

where F_n with $n \in \{0, 1, 2, 3, 4, 5, 6, b\}$ is the corresponding coefficient (see Appendix B). The coherent output spectrum versus the perturbation δ_s is given by

$$T_g = \frac{\langle\hat{d}_b^\dagger\hat{d}_b\rangle}{|\alpha|^2} = \frac{|F_0|^2}{|\alpha|^2} = \left|1 + \kappa_{ex}\frac{i\Delta' + \kappa + g'\sin\varphi}{\lambda_+\lambda_-}\right|^2. \tag{11}$$

According to Eq. (11), the eigenfrequencies can be extracted by fitting the output spectrum with

$$T_{fit} = \left|1 + R_1\frac{\Delta' + iR_2}{(\Delta' + R_3 + iR_4)(\Delta' + R_5 + iR_6)}\right|^2, \tag{12}$$

where R_j with $j \in \{1, 2, 3, 4, 5, 6\}$ presents the fitting parameter normalized to κ_{ex}. The retrieved eigenfrequencies $\tilde{\lambda}_+$ and $\tilde{\lambda}_-$ are related to these parameters as $\mathrm{Re}(\tilde{\lambda}_+) = R_3$, $\mathrm{Im}(\tilde{\lambda}_+) = R_4$, $\mathrm{Re}(\tilde{\lambda}_-) = R_5$, and $\mathrm{Im}(\tilde{\lambda}_-) = R_6$. Note that these fitting functions are distinct from that for the non-Hermitian magneto-optical effect [64]. In Ref. [64], the two coupled modes are orthogonal in polarization and the transmission spectrum can be simply fitted with the sum of two Lorentzian profiles. In contrast, the reflected fields $\hat{a}_{out,1}$ and $\hat{a}_{out,2}$ in this NHMI are nonorthogonal and interfere to form the complicated output field $\hat{d}_b$. Thus, the output spectrum of the NHMI cannot be expressed as a simple sum of two Lorentzian functions.

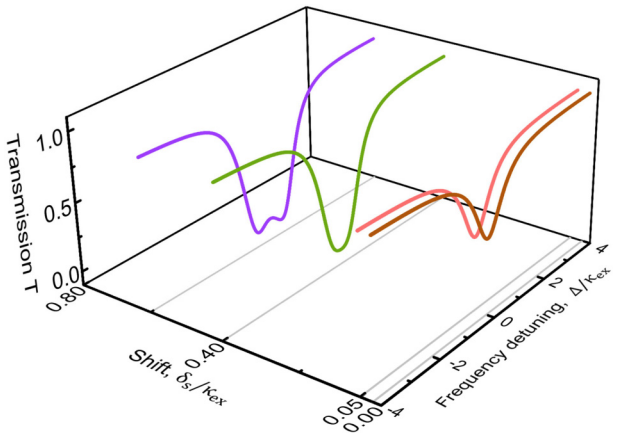


FIG. 2. Transmission vs normalized frequency detuning Δ/κ_{ex} for different frequency shifts δ_s. The EP occurs at $\delta_s = 0.05\kappa_{ex}$. Other parameters are set to $\theta = \pi/4$, $\varphi = \pi/2$, $\kappa_{ex,3} = 0.2\kappa_{ex}$, and $\kappa_{ex,4} = 0$.

III. RESULTS

The output spectra of the NHMI for different perturbations δ_s are presented in Fig. 2. An EP appears at $\delta_s^{EP} = 0.05\kappa_{ex}$. The output spectrum exhibits a single resonance peak when $\delta_s < 0.40\kappa_{ex}$ and splits into two peaks when $\delta_s > 0.40\kappa_{ex}$—see the purple curve at $\delta_s = 0.60\kappa_{ex}$, for example.

The real parts of the eigenfrequencies are shown in Fig. 3(a). In the conventional HMI, the real parts of eigenfrequencies, $\lambda'_{\pm}$, split linearly with perturbation, see the blue and red dashed lines. By contrast, the NHMI exhibits typical non-Hermitian behavior: the eigenfrequencies remain degenerate before the EP and undergo a square-root splitting beyond it. The retrieved eigenfrequencies, $\mathrm{Re}[\tilde{\lambda}_{\pm}]$, are in excellent agreement with the numerical results, $\mathrm{Re}[\lambda_{\pm}]$. The corresponding eigenfrequency splitting as a response is plotted in Fig. 3(b). The NHMI displays a square-root dependence near the EP, yielding a larger splitting for a small signal ε on top of the bias δ_s^{EP}. The dynamical response of MIs is quantified by

$$R(g) = \frac{\partial \Delta\lambda}{\partial \delta_s} = \frac{2\delta_s}{\sqrt{\delta_s^2 - g^2}}. \tag{13}$$

As shown in Fig. 3(c), for a perturbation $\delta_s = \delta_s^{EP} + \varepsilon$, the NHMI exhibits a dynamic response enhanced by a factor $\propto 1/\sqrt{\varepsilon}$, indicating a dramatic enhancement for a small signal. For example, for small signals $\varepsilon = 10^{-6}\kappa_{ex}$ and $10^{-8}\kappa_{ex}$, the dynamic response reaches $R \approx 316$ and 3162, corresponding to an enhancement of 158 and 1581, respectively, when $g \neq 0$.

The metrological performance of the MIs with mechanical vibration is generally constrained by quantum vacuum noise and Brownian noise. In quantum metrology, the QFI provides a fundamental measure for quantifying the ultimate precision limit of parameter estimation [94–97]. According to the quantum Cramér-Rao bound, the variance of an unbiased estimator of the signal parameter δ_s satisfies $\mathrm{Var}(\delta_s) \geqslant 1/F_Q(\delta_s)$, where $F_Q(\delta_s)$ denotes the QFI associated with the estimation of δ_s. We use a coherent probe laser field. The output field remains Gaussian under the linearized dynamics. Therefore, the QFI can be evaluated with the covariance matrix $\mathbf{V}$. The sensitivity

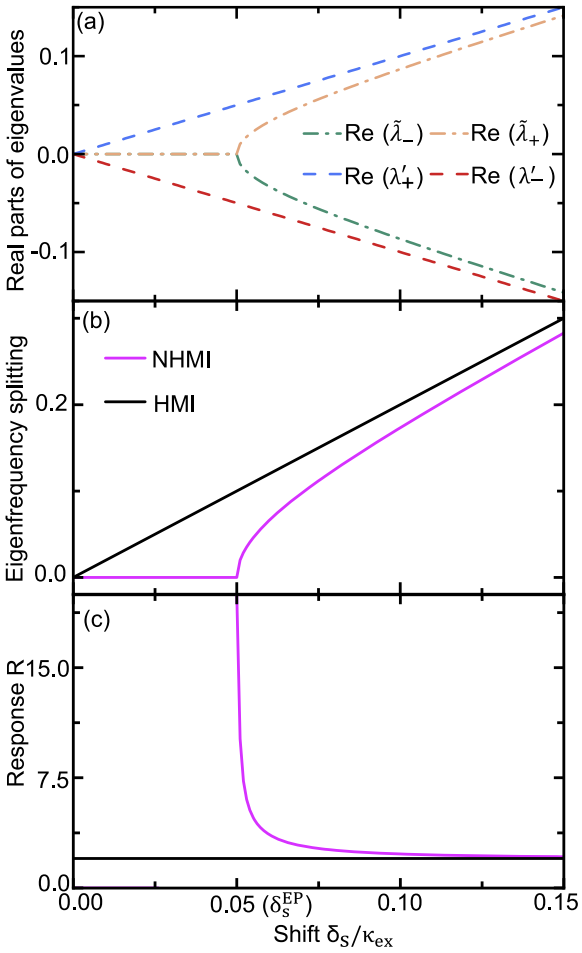


FIG. 3. Comparison of the performance of the NHMI and the HMI. (a) Real parts of the system eigenfrequencies. $\mathrm{Re}(\tilde{\lambda}_{\pm})$ is the fitted values extracted from the transmission spectra. $\mathrm{Re}(\lambda'_{\pm})$ denotes the real parts of eigenfrequencies for HMI. (b) Eigenfrequency splitting, $\Delta\lambda = \mathrm{Re}(\lambda_+) - \mathrm{Re}(\lambda_-)$, as a function of δ_s. The purple curve is for the NHMI and the black curve for the HMI. (c) Dynamic response vs δ_s. For the NHMI, the parameters are set as follows: $\theta = \pi/4$, $\varphi = \pi/2$, and $\kappa_{ex,3} = 0.2\kappa_{ex}$. For the HMI, the parameters are set as $\theta = \pi/4$, $\varphi = \pi/2$, and $\kappa'_{ex} = 1.1\kappa_{ex}$ in order to make the effective losses κ_a and κ_b equal to those in the NHMI.

is determined by the amplitude vector $\boldsymbol{\mu}_{out}$ (see Appendix C) and the covariance matrix of the output field [98]. The QFI for both the NHMI and the HMI can be evaluated by [94–98]

$$F_Q = \left(\frac{d\boldsymbol{\mu}_{out}}{d\delta_s}\right)^T \mathbf{V}^{-1} \left(\frac{\mathrm{d}\boldsymbol{\mu}_{out}}{\mathrm{d}\delta_s}\right) = \frac{2}{\sum_{i=1}^{6} |F_i|^2 + |F_b|^2(2n_{th}+1)} \left|\frac{dF_0}{d\delta_s}\right|^2. \tag{14}$$

The coefficients F_0, F_b, and F_i are different for the NHMI and the HMI. When Brownian noise dominates over quantum vacuum noise, the QFI enhancement or the sensitivity enhancement approaches a constant value.

As shown in Fig. 4(a), for $g_{om} \lesssim 0.01\kappa_{ex}$, the QFI of the NHMI consistently exceeds that of the HMI, indicating superior metrological performance. We quantify this advantage by defining the enhancement factor $E_F = F_Q^{NHMI}/F_Q^{HMI}$. For

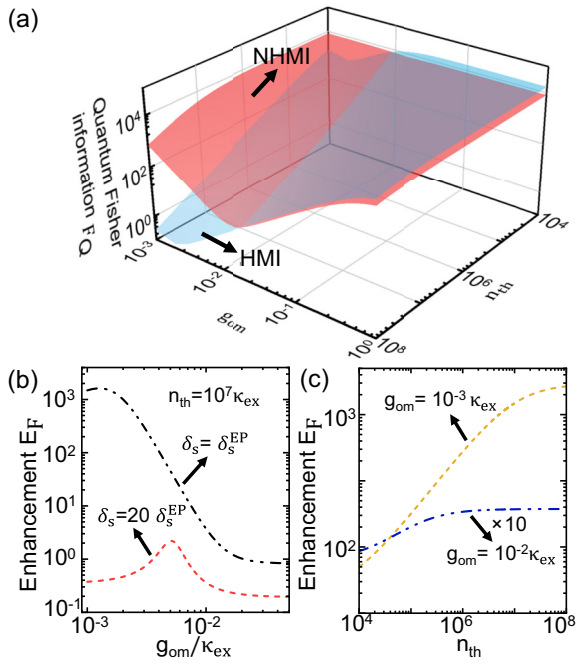


FIG. 4. (a) QFI vs the optomechanical coupling strength $g_{\rm om}$ and the thermal phonon number $n_{\rm th}$. The red and blue surfaces correspond to the NHMI and HMI, respectively. (b) QFI enhancement as a function of $g_{\rm om}$ for $n_{\rm th} = 10^7$ at $\delta_{\rm s} = \delta_{\rm s}^{\rm EP}$ and $\delta_{\rm s} = 20\delta_{\rm s}^{\rm EP}$. (c) QFI enhancement as a function of $n_{\rm th}$ for $g_{\rm om} = 10^{-2}\kappa_{\rm ex}$ and $g_{\rm om} = 10^{-3}\kappa_{\rm ex}$. The curve for $g_{\rm om} = 10^{-2}\kappa_{\rm ex}$ is scaled by a factor of 10. Other parameters are $\theta = \pi/4$, $\varphi = \pi/2$, $\Delta = 0$, $\omega_{\rm b} = 0.1\kappa_{\rm ex}$, $\delta_{\rm s} = 0.05\kappa_{\rm ex}$, $\gamma_{\rm m} = 10^{-4}\kappa_{\rm ex}$, $\kappa_{\rm ex,3} = 0.2\kappa_{\rm ex}$, and $\kappa_{\rm ex,4} = 0$.

$n_{\rm th} = 10^7$ as shown in Fig. 4(b), the QFI is enhanced by a factor of $E_{\rm F} = 1620$ at $g_{\rm om} = 1.3 \times 10^{-3}\kappa_{\rm ex}$. The enhancement drops below unity for $g_{\rm om} > 2.1 \times 10^{-2}\kappa_{\rm ex}$. When the system is operated away from the EP, with $\delta_{\rm s} = 20\delta_{\rm s}^{\rm EP}$, the enhancement rapidly decreases, reaching a maximum value of only 2.2 at $g_{\rm om} = 5.1 \times 10^{-3}\kappa_{\rm ex}$. For a very large optomechanical coupling, e.g., $g_{\rm om} = 10^{-2}\kappa_{\rm ex}$, which is difficult to access in experiments, $E_{\rm F}$ saturates at a small value 3.7. For a weak optomechanical coupling strength of $g_{\rm om} = 10^{-3}\kappa_{\rm ex}$ accessible under most experimental conditions, $E_{\rm F}$ increases with $n_{\rm th}$ and approaches a saturated value of 2600 for $n_{\rm th} \gtrsim 7.6 \times 10^7$, see Fig. 4(c), because the response improves faster than the noise amplification. This implies a sensitivity enhancement more than three orders.

Although the performance of optical interferometers can be enhanced by exploiting quantum resources such as squeezed light, and remarkable experimental progress has been achieved in this direction, the underlying enhancement mechanism is fundamentally different from that of the proposed scheme [7,21–24]. Squeezed-light interferometry improves the measurement sensitivity by reducing quantum noise through the generation, injection, and preservation of nonclassical optical states, whereas the present approach exploits the enhanced parameter-dependent response arising from the non-Hermitian dynamics of an anti-PT-symmetric interferometric platform. The highest reported optical squeezing level has reached 18 dB [99], while large-scale interferometric experiments, such as gravitational-wave detectors, have demonstrated a sensitivity improvement of approximately 3 dB through the use of squeezed light [7]. By contrast, under experimentally accessible conditions, our scheme predicts an enhancement of the QFI of up to 32 dB, defined as $10\log_{10}(E_{\rm F})$. We emphasize that this quantity characterizes the enhancement of the QFI and is not directly equivalent to the experimentally realized noise reduction in squeezed-light interferometry. Nevertheless, the result indicates that the proposed non-Hermitian system can provide a substantial metrological enhancement without relying on nonclassical resource. A further practical advantage of the proposed scheme is that it requires only coherent-light injection, which is generally easier to prepare, stabilize, and integrate into existing interferometric platforms than squeezed light. The scheme avoids the additional experimental overhead associated with the generation, injection, and phase stabilization of squeezed states. Importantly, all key ingredients of the scheme, including Fabry-Pérot cavities, beam splitters, and reservoir-engineered dissipative coupling, are available with current photonic technologies. The dissipative coupling can be engineered through a controlled imbalance in the external losses of the two cavities. These features make the proposed scheme compatible with existing experimental platforms and provide a feasible route toward EP-enhanced precision measurements.

Several practical challenges exist in possible experimental implementations. First, the losses introduced by the cavity mirrors must be precisely engineered to realize the required dissipative coupling strength for a given signal and thereby satisfy the EP condition. Second, intrinsic cavity losses should remain sufficiently small to ensure that the mirror-induced dissipative coupling can be accurately controlled. Third, mechanical vibrations, thermal drifts, and other environmental perturbations may shift the system away from the desired operating point and therefore require appropriate stabilization and feedback. Finally, operation in the vicinity of the EP inherently restricts the dynamic response range, leading to a trade-off between enhanced sensitivity and measurement bandwidth.

IV. CONCLUSION

We have proposed a light cross to incorporate non-Hermiticity into a MI via reservoir engineering. The proposed NHMI exhibits a square-root eigenfrequency splitting in response to perturbation near the EP. The NHMI achieves a three-order-higher QFI in comparison with the HMI, when both quantum vacuum and Brownian noises are considered. This light cross enables an opportunity for EP-enhanced interferometric sensing with an ultrahigh sensitivity.

ACKNOWLEDGMENTS

This work was supported by the National Natural Science Foundation of China (Grants No. U25A6008, No. U25A60082, and No. 92365107), the Innovation Program for Quantum Science and Technology (Grant No. 2021ZD0301400), the National University of Defense Technology Independent Innovation Science Foundation (24-ZZCX-JDZ-11), the China Postdoctoral Science Foundation

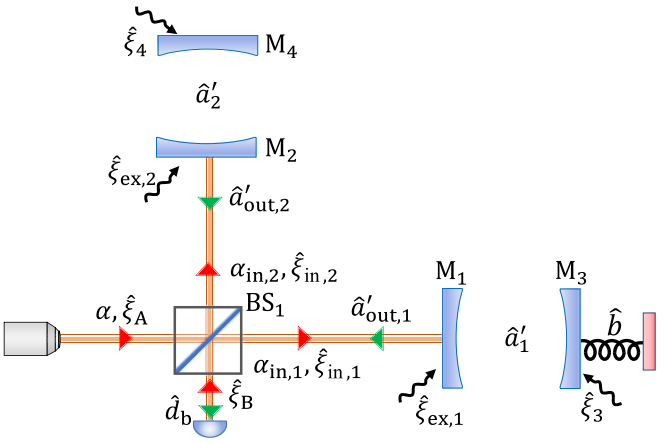


FIG. 5. Schematic of the HMI. A coherent probe field is injected from the left and is split by BS_1 into two paths, driving cavity modes $\hat{a}'_1$ and $\hat{a}'_2$ via mirrors M_1 and M_2. $\hat{\xi}_{ex,1}$, $\hat{\xi}_{ex,2}$, $\hat{\xi}_3$, and $\hat{\xi}_4$ denote quantum noises entering the system via the mirrors. $\hat{\xi}_{in,1}$ and $\hat{\xi}_{in,2}$ denote quantum noises entering the system via the beam splitter. The vibration mode $\hat{b}$, suffering thermal noise, couples to $\hat{a}'_1$ via mirror M_3.

(Grant No. 2023M731613), the Jiangsu Funding Program for Excellent Postdoctoral Talent (Grant No. 2023ZB708), and the Natural Science Foundation of Jiangsu Province, Major Project.

DATA AVAILABILITY

There are no publicly available research data or software supporting this manuscript. Requests for further information or data should be sent to the authors.

APPENDIX A: THE HAMILTONIAN OF THE NHMI AND THE HMI

In this section, we derive the system Hamiltonian and elucidate the emergence of the effective coupling between cavity modes $\hat{a}_1$ and $\hat{a}_2$. In a conventional Michelson interferometer, hereafter referred to as the Hermitian Michelson interferometer (HMI), the two cavity modes evolve independently without any direct interaction, as illustrated in Fig. 5. In contrast, in our non-Hermitian Michelson interferometer (NHMI), an effective coupling between $\hat{a}_1$ and $\hat{a}_2$ is engineered via a shared reservoir. As illustrated in Fig. 1, the beam splitter BS_2 transforms the primary modes $\hat{a}_1$ and $\hat{a}_2$ into auxiliary supermodes $\hat{a}_3$ and $\hat{a}_4$ with the relations

$$\begin{aligned}\hat{a}_3 &= \cos\theta'\,\hat{a}_1 - ie^{-i\varphi'}\sin\theta'\,\hat{a}_2,\\ \hat{a}_4 &= \cos\theta'\,\hat{a}_2 - ie^{i\varphi'}\sin\theta'\,\hat{a}_1,\end{aligned} \tag{A1}$$

where $\cos\theta'$ and $\sin\theta'$ are reflection and transmission amplitudes of the BS_2, respectively, and φ' is the relative phase between the two transmitted modes. These supermodes couple to a common thermal reservoir, thereby mediating an indirect interaction between the original cavity modes. The dissipation rates of the auxiliary supermodes are denoted by $\kappa_{ex,3}$ and $\kappa_{ex,4}$, respectively. When $\kappa_{ex,3} \neq \kappa_{ex,4}$, an effective non-Hermitian coupling between $\hat{a}_1$ and $\hat{a}_2$ emerges. For comparison, in the HMI, the two cavities are identical and independent, with $\kappa'_{ex,1} = \kappa'_{ex,2}$ and $\kappa'_{ex,3} = \kappa'_{ex,4} = 0$, such that no coupling is induced between the two modes.

We first focus on the HMI with no coupling between modes $\hat{a}'_1$ and $\hat{a}'_2$. Thus, the effective Hamiltonian $\hat{H}_{H,s}$ of the HMI can be described as

$$\begin{aligned}\hat{H}_{H,s} = &\left(\omega_0 + \delta_s - i\frac{\kappa'_{ex,1}}{2}\right)\hat{a}'^{\dagger}_1\hat{a}'_1 + \left(\omega_0 - \delta_s - i\frac{\kappa'_{ex,2}}{2}\right)\hat{a}'^{\dagger}_2\hat{a}'_2\\ &+ i\sqrt{\kappa'_{ex,1}}(\alpha^*_{in,1}\hat{a}'_1 - \hat{a}'^{\dagger}_1\alpha_{in,1})\\ &+ i\sqrt{\kappa'_{ex,2}}(\alpha^*_{in,2}\hat{a}'_2 - \hat{a}'^{\dagger}_2\alpha_{in,2}),\end{aligned} \tag{A2}$$

where ω_0 denotes the effective resonant frequency of cavity modes $\hat{a}'_1$ and $\hat{a}'_2$, and δ_s represents the frequency shift induced by a perturbation of the cavity length. Here, we consider the losses, $\kappa'_{ex,1}$ and $\kappa'_{ex,2}$, induced by the cavity mirrors. We neglect the intrinsic losses of cavities modes, as well as the quantum jump terms. This approximation is well justified in the regime of strong coherent driving with a large photon number. $\alpha_{in,1}$ and $\alpha_{in,2}$ denote the coherent amplitudes driving the cavity modes after splitting by the beam splitter BS_1. They are related to the input coherent amplitude α through [92]

$$\alpha_{in,1} = \cos\theta\,\alpha, \quad \alpha_{in,2} = -ie^{-i\varphi}\sin\theta\,\alpha, \tag{A3}$$

where $\cos\theta$ and $\sin\theta$ are reflection and transmission amplitudes of the BS_1, respectively, and φ is the relative phase between the two transmitted modes.

The vacuum fluctuations coupled into the system via BS_1 can be described by

$$\begin{aligned}\hat{\xi}_{in,1} &= \cos\theta\,\hat{\xi}_A - ie^{i\varphi}\sin\theta\,\hat{\xi}_B,\\ \hat{\xi}_{in,2} &= \cos\theta\,\hat{\xi}_B - ie^{-i\varphi}\sin\theta\,\hat{\xi}_A,\end{aligned} \tag{A4}$$

where $\hat{\xi}_A$ and $\hat{\xi}_B$ denote the vacuum noise operators associated with the input ports of BS_1.

In this system, vacuum noise operators $\hat{\xi}_1$, $\hat{\xi}_2$, $\hat{\xi}_3$, and $\hat{\xi}_4$ enter the cavity through the corresponding mirrors, where $\hat{\xi}_1 = \hat{\xi}_{in,1} + \hat{\xi}_{ex,1}$ and $\hat{\xi}_2 = \hat{\xi}_{in,2} + \hat{\xi}_{ex,2}$. Here, $\hat{\xi}_{ex,1}$ and $\hat{\xi}_{ex,2}$ describe the vacuum noise operators that directly couple to the cavity modes. In addition, we consider that a mechanical mode $\hat{b}$ couples to the $\hat{a}'_1$ via the cavity mirror M_3, with frequency ω_b, damping rate γ_m, and optomechanical coupling strength g_{om}. The mechanical mode $\hat{b}$ is driven by a thermal noise operator $\hat{b}_{in}$, which satisfies $\langle\hat{b}^{\dagger}_{in}\hat{b}_{in}\rangle = n_{th}$, where n_{th} is the thermal excited phonon number. The corresponding noise contribution can be described by the Hamiltonian $\hat{H}_{H,n}$,

$$\begin{aligned}\hat{H}_{H,n} = &\,i\sqrt{\kappa'_{ex,1}}(\hat{\xi}^{\dagger}_1\hat{a}'_1 - \hat{a}'^{\dagger}_1\hat{\xi}_1) + i\sqrt{\kappa'_{ex,2}}(\hat{\xi}^{\dagger}_2\hat{a}'_2 - \hat{a}'^{\dagger}_2\hat{\xi}_2)\\ &+ i\sqrt{\kappa'_{ex,3}}(\hat{\xi}^{\dagger}_3\hat{a}'_1 - \hat{a}'^{\dagger}_1\hat{\xi}_3) + i\sqrt{\kappa'_{ex,4}}(\hat{\xi}^{\dagger}_4\hat{a}'_2 - \hat{a}'^{\dagger}_2\hat{\xi}_4)\\ &+ \left(\omega_b - i\frac{\gamma_m}{2}\right)\hat{b}'^{\dagger}\hat{b}' + g_{om}\hat{a}'^{\dagger}_1\hat{a}'_1(\hat{b}'^{\dagger} + \hat{b}')\\ &+ i\sqrt{\gamma_m}(\hat{b}^{\dagger}_{in}\hat{b}' - \hat{b}'^{\dagger}\hat{b}_{in}).\end{aligned} \tag{A5}$$

In contrast to the HMI, the effective system Hamiltonian $\hat{H}_{NH,s}$ of the NHMI is constructed from two cavity modes, $\hat{a}_1$

and $\hat{a}_2$, and two supermodes, $\hat{a}_3$ and $\hat{a}_4$, and is given by

$$\begin{aligned}\hat{H}_{\mathrm{NH,s}} &= \Big(\omega_0+\delta_\mathrm{s}-i\frac{\kappa_{\mathrm{ex},1}}{2}\Big)\hat{a}_1^\dagger\hat{a}_1+i\sqrt{\kappa_{\mathrm{ex},1}}(\alpha_{\mathrm{in},1}^*\hat{a}_1-\hat{a}_1^\dagger\alpha_{\mathrm{in},1})\\&+\Big(\omega_0-\delta_\mathrm{s}-i\frac{\kappa_{\mathrm{ex},2}}{2}\Big)\hat{a}_2^\dagger\hat{a}_2+i\sqrt{\kappa_{\mathrm{ex},2}}(\alpha_{\mathrm{in},2}^*\hat{a}_2-\hat{a}_2^\dagger\alpha_{\mathrm{in},2})\\&-i\frac{\kappa_{\mathrm{ex},3}}{2}\hat{a}_3^\dagger\hat{a}_3-i\frac{\kappa_{\mathrm{ex},4}}{2}\hat{a}_4^\dagger\hat{a}_4. \qquad \text{(A6)}\end{aligned}$$

The noise operators in the NHMI are similar to those in the HMI. In the HMI, the vacuum noise operators $\hat{\xi}_1$ and $\hat{\xi}_3$ both couple to cavity mode $\hat{a}_1'$, while $\hat{\xi}_2$ and $\hat{\xi}_4$ couple to cavity mode $\hat{a}_2'$. In contrast, in the NHMI, the noise couplings are redistributed: the vacuum noise operators $\hat{\xi}_1$ and $\hat{\xi}_3$ couple to $\hat{a}_1$ and $\hat{a}_3$, respectively, whereas $\hat{\xi}_2$ and $\hat{\xi}_4$ couple to $\hat{a}_2$ and $\hat{a}_4$, respectively. In addition, mechanical mode $\hat{b}$ couples to supermode $\hat{a}_4$ via cavity mirror M_3. As a result, the noise contributions in the NHMI can be described by the Hamiltonian $\hat{H}_{\mathrm{NH,n}}$,

$$\begin{aligned}\hat{H}_{\mathrm{NH,n}} &= i\sqrt{\kappa_{\mathrm{ex},1}}(\hat{\xi}_1^\dagger\hat{a}_1-\hat{a}_1^\dagger\hat{\xi}_1)+i\sqrt{\kappa_{\mathrm{ex},2}}(\hat{\xi}_2^\dagger\hat{a}_2-\hat{a}_2^\dagger\hat{\xi}_2)\\&+i\sqrt{\kappa_{\mathrm{ex},3}}(\hat{\xi}_3^\dagger\hat{a}_3-\hat{a}_3^\dagger\hat{\xi}_3)+i\sqrt{\kappa_{\mathrm{ex},4}}(\hat{\xi}_4^\dagger\hat{a}_4-\hat{a}_4^\dagger\hat{\xi}_4)\\&+\Big(\omega_\mathrm{b}-i\frac{\gamma_\mathrm{m}}{2}\Big)\hat{b}^\dagger\hat{b}+g_\mathrm{om}\hat{a}_4^\dagger\hat{a}_4(\hat{b}^\dagger+\hat{b})\\&+i\sqrt{\gamma_\mathrm{m}}(\hat{b}_\mathrm{in}^\dagger\hat{b}-\hat{b}^\dagger\hat{b}_\mathrm{in}). \qquad \text{(A7)}\end{aligned}$$

By substituting Eq. (A1) into Eqs. (A6) and (A7), we obtain the effective system Hamiltonian $\hat{H}'_{\mathrm{NH,s}}$ and the noise Hamiltonian $\hat{H}'_{\mathrm{NH,n}}$ that involve only cavity modes $\hat{a}_1$ and $\hat{a}_2$,

$$\begin{aligned}\hat{H}'_{\mathrm{NH,s}} &= \left(\omega_0+\delta_\mathrm{s}-i\frac{\kappa_{\mathrm{ex},1}+\cos^2\theta'\,\kappa_{\mathrm{ex},3}+\sin^2\theta'\,\kappa_{\mathrm{ex},4}}{2}\right)\hat{a}_1^\dagger\hat{a}_1\\&+\left(\omega_0-\delta_\mathrm{s}-i\frac{\kappa_{\mathrm{ex},2}+\sin^2\theta'\,\kappa_{\mathrm{ex},3}+\cos^2\theta'\,\kappa_{\mathrm{ex},4}}{2}\right)\hat{a}_2^\dagger\hat{a}_2\\&+\frac{\kappa_{\mathrm{ex},4}-\kappa_{\mathrm{ex},3}}{2}\sin\theta'\cos\theta'\,(e^{-i\varphi'}\hat{a}_1^\dagger\hat{a}_2-e^{i\varphi'}\hat{a}_2^\dagger\hat{a}_1)\\&+i\sqrt{\kappa_{\mathrm{ex},1}}(\alpha_{\mathrm{in},1}^*\hat{a}_1-\hat{a}_1^\dagger\alpha_{\mathrm{in},1})\\&+i\sqrt{\kappa_{\mathrm{ex},2}}(\alpha_{\mathrm{in},2}^*\hat{a}_2-\hat{a}_2^\dagger\alpha_{\mathrm{in},2}),\\\hat{H}'_{\mathrm{NH,n}} &= i\sqrt{\kappa_{\mathrm{ex},1}}(\hat{\xi}_1^\dagger\hat{a}_1-\hat{a}_1^\dagger\hat{\xi}_1)+i\sqrt{\kappa_{\mathrm{ex},2}}(\hat{\xi}_2^\dagger\hat{a}_2-\hat{a}_2^\dagger\hat{\xi}_2)\\&+i\cos\theta'\sqrt{\kappa_{\mathrm{ex},3}}(\hat{\xi}_3^\dagger\hat{a}_1-\hat{a}_1^\dagger\hat{\xi}_3)\\&+\sin\theta'\sqrt{\kappa_{\mathrm{ex},3}}(e^{-i\varphi'}\hat{\xi}_3^\dagger\hat{a}_2+e^{i\varphi'}\hat{a}_2^\dagger\hat{\xi}_3)\\&+i\cos\theta'\sqrt{\kappa_{\mathrm{ex},4}}(\hat{\xi}_4^\dagger\hat{a}_2-\hat{a}_2^\dagger\hat{\xi}_4)\\&+\sin\theta'\sqrt{\kappa_{\mathrm{ex},4}}(e^{i\varphi'}\hat{\xi}_4^\dagger\hat{a}_1+e^{-i\varphi'}\hat{a}_1^\dagger\hat{\xi}_4)\\&+\Big(\omega_\mathrm{b}-i\frac{\gamma_\mathrm{m}}{2}\Big)\hat{b}^\dagger\hat{b}+i\sqrt{\gamma_\mathrm{m}}(\hat{b}_\mathrm{in}^\dagger\hat{b}-\hat{b}^\dagger\hat{b}_\mathrm{in})\\&+g_\mathrm{om}[\cos^2\theta'\,\hat{a}_2^\dagger\hat{a}_2+\sin^2\theta'\,\hat{a}_1^\dagger\hat{a}_1\\&+i\sin\theta'\cos\theta'(e^{-i\varphi'}\hat{a}_1^\dagger\hat{a}_2-e^{i\varphi'}\hat{a}_2^\dagger\hat{a}_1)](\hat{b}^\dagger+\hat{b}). \qquad \text{(A8)}\end{aligned}$$

For a balanced BS_2 with $\theta'=\pi/4$ and $\varphi'=\pi/2$, the Hamiltonians in Eq. (A8) can be simplified to

$$\begin{aligned}\hat{H}''_{\mathrm{NH,s}} &= (\omega_0+\delta_\mathrm{s}-i\kappa_1)\hat{a}_1^\dagger\hat{a}_1+i\sqrt{\kappa_{\mathrm{ex},1}}(\alpha_{\mathrm{in},1}^*\hat{a}_1-\hat{a}_1^\dagger\alpha_{\mathrm{in},1})\\&+(\omega_0-\delta_\mathrm{s}-i\kappa_2)\hat{a}_2^\dagger\hat{a}_2+i\sqrt{\kappa_{\mathrm{ex},2}}(\alpha_{\mathrm{in},2}^*\hat{a}_2-\hat{a}_2^\dagger\alpha_{\mathrm{in},2})\\&-ig(\hat{a}_1^\dagger\hat{a}_2+\hat{a}_2^\dagger\hat{a}_1),\end{aligned}$$

$$\begin{aligned}\hat{H}''_{\mathrm{NH,n}} &= i\sqrt{\kappa_{\mathrm{ex},1}}(\hat{\xi}_1^\dagger\hat{a}_1-\hat{a}_1^\dagger\hat{\xi}_1)+i\sqrt{\kappa_{\mathrm{ex},2}}(\hat{\xi}_2^\dagger\hat{a}_2-\hat{a}_2^\dagger\hat{\xi}_2)\\&+i\sqrt{\frac{\kappa_{\mathrm{ex},3}}{2}}(\hat{\xi}_3^\dagger\hat{a}_1-\hat{a}_1^\dagger\hat{\xi}_3)+i\sqrt{\frac{\kappa_{\mathrm{ex},3}}{2}}(\hat{a}_2^\dagger\hat{\xi}_3-\hat{\xi}_3^\dagger\hat{a}_2)\\&+i\sqrt{\frac{\kappa_{\mathrm{ex},4}}{2}}(\hat{\xi}_4^\dagger\hat{a}_2-\hat{a}_2^\dagger\hat{\xi}_4)+i\sqrt{\frac{\kappa_{\mathrm{ex},4}}{2}}(\hat{\xi}_4^\dagger\hat{a}_1-\hat{a}_1^\dagger\hat{\xi}_4)\\&+\Big(\omega_\mathrm{b}-i\frac{\gamma_\mathrm{m}}{2}\Big)\hat{b}^\dagger\hat{b}+i\sqrt{\gamma_\mathrm{m}}(\hat{b}_\mathrm{in}^\dagger\hat{b}-\hat{b}^\dagger\hat{b}_\mathrm{in})\\&+\frac{g_\mathrm{om}}{2}(\hat{a}_1^\dagger+\hat{a}_2^\dagger)(\hat{a}_1+\hat{a}_2)(\hat{b}^\dagger+\hat{b}), \qquad \text{(A9)}\end{aligned}$$

where the effective losses of modes $\hat{a}_1$ and $\hat{a}_2$ are $\kappa_1=(2\kappa_{\mathrm{ex},1}+\kappa_{\mathrm{ex},3}+\kappa_{\mathrm{ex},4})/4$ and $\kappa_2=(2\kappa_{\mathrm{ex},2}+\kappa_{\mathrm{ex},3}+\kappa_{\mathrm{ex},4})/4$, respectively, and $g=(\kappa_{\mathrm{ex},4}-\kappa_{\mathrm{ex},3})/4$ is the effective coupling rate between $\hat{a}_1$ and $\hat{a}_2$ that has the same definition as reservoir engineering.

Throughout, we set $\kappa_{\mathrm{ex},4}=0$ for both cases. To ensure equal effective losses, we set $\kappa_{\mathrm{ex},1}=\kappa_{\mathrm{ex},2}=\kappa_\mathrm{ex}$ in the NHMI and choose $\kappa'_{\mathrm{ex},1}=\kappa'_{\mathrm{ex},2}=(\kappa_{\mathrm{ex},1}+\kappa_{\mathrm{ex},2}+\kappa_{\mathrm{ex},3}+\kappa_{\mathrm{ex},4})/2$ in the HMI.

APPENDIX B: THE OUTPUT MODE OF THE NHMI

In this section, we derive the analytical steady-state solutions for the cavity mode operators and the corresponding output field of MIs. The resulting expressions explicitly present the output mode as a function of the mode coupling g, the frequency shift δ_s, the relative phase φ of BS_1, and noise contributions.

In a rotating frame with respect to cavity mode $\hat{a}_1$, the quantum Langevin equations corresponding to the Hamiltonians in Eq. (A9) are given by

$$\begin{aligned}\frac{d\hat{b}}{dt} &= \Big(-i\omega_\mathrm{b}-\frac{\gamma_\mathrm{m}}{2}\Big)\hat{b}-i\frac{g_\mathrm{om}}{2}(\hat{a}_1^\dagger+\hat{a}_2^\dagger)(\hat{a}_1+\hat{a}_2)-\sqrt{\gamma_\mathrm{m}}\hat{b}_\mathrm{in},\\\frac{d\hat{a}_1}{dt} &= \Big[-i\Delta-\kappa_1-i\frac{g_\mathrm{om}}{2}(\hat{b}^\dagger+\hat{b})\Big]\hat{a}_1-g'\hat{a}_2\\&-\sqrt{\kappa_{\mathrm{ex},1}}(\alpha_{\mathrm{in},1}+\hat{\xi}_1)-\sqrt{\frac{\kappa_{\mathrm{ex},3}}{2}}\hat{\xi}_3-\sqrt{\frac{\kappa_{\mathrm{ex},4}}{2}}\hat{\xi}_4,\\\frac{d\hat{a}_2}{dt} &= \Big[-i\Delta-\kappa_2-i\frac{g_\mathrm{om}}{2}(\hat{b}^\dagger+\hat{b})\Big]\hat{a}_2-g'\hat{a}_1\\&-\sqrt{\kappa_{\mathrm{ex},2}}(\alpha_{\mathrm{in},2}+\hat{\xi}_2)+\sqrt{\frac{\kappa_{\mathrm{ex},3}}{2}}\hat{\xi}_3-\sqrt{\frac{\kappa_{\mathrm{ex},4}}{2}}\hat{\xi}_4, \qquad \text{(B1)}\end{aligned}$$

where $\Delta=\omega_0-\omega_\mathrm{p}$ and $g'=g+ig_\mathrm{om}/2(\hat{b}^\dagger+\hat{b})$.

To obtain the steady-state solution for the output mode $\hat{d}_\mathrm{b}$ in the presence of thermal noise, we linearize cavity modes $\hat{a}_1$ and $\hat{a}_2$ and mechanical mode $\hat{b}$ as

$$\hat{a}_1=\alpha_1+\delta\hat{a}_1,\quad \hat{a}_2=\alpha_2+\delta\hat{a}_2,\quad \hat{b}=\alpha_\mathrm{b}+\delta\hat{b}, \qquad \text{(B2)}$$

where $\alpha_{1,2}=\langle\hat{a}_{1,2}\rangle$ and $\alpha_\mathrm{b}=\langle\hat{b}\rangle$ denote the mean-field amplitudes and $\delta\hat{a}_{1,2}$ and $\delta\hat{b}$ represent the corresponding fluctuation operators.

The Langevin equations in Eq. (B1) can be decomposed into two parts. One corresponds to the mean-field dynamics,

$$\begin{aligned}
\frac{d\alpha_{\rm b}}{dt} &= \Big(-i\omega_{\rm b}-\frac{\gamma_{\rm m}}{2}\Big)\alpha_{\rm b}-i\frac{g_{\rm om}}{2}(|\alpha_1|^2+|\alpha_2|^2+\alpha_1^*\alpha_2+\alpha_2^*\alpha_1),\\
\frac{d\alpha_1}{dt} &= [-i(\Delta'+\delta_{\rm s})-\kappa_1]\alpha_1-g'\alpha_2-\sqrt{\kappa_{\rm ex,1}}\alpha_{\rm in,1},\\
\frac{d\alpha_2}{dt} &= [-i(\Delta'-\delta_{\rm s})-\kappa_2]\alpha_1-g'\alpha_1-\sqrt{\kappa_{\rm ex,2}}\alpha_{\rm in,2},
\end{aligned} \tag{B3}$$

and the other corresponds to the fluctuations,

$$\begin{aligned}
\frac{d\delta\hat{a}_1}{dt} &= [-i(\Delta+\delta_{\rm s})-\kappa_1]\delta\hat{a}_1-iG\delta\hat{b}-g'\delta\hat{a}_2-\sqrt{\kappa_{\rm ex,1}}\hat{\xi}_1\\
&\quad-\sqrt{\frac{\kappa_{\rm ex,3}}{2}}\hat{\xi}_3-\sqrt{\frac{\kappa_{\rm ex,4}}{2}}\hat{\xi}_4,\\
\frac{d\delta\hat{a}_2}{dt} &= [-i(\Delta-\delta_{\rm s})-\kappa_2]\delta\hat{a}_2-iG\delta\hat{b}-g'\delta\hat{a}_1-\sqrt{\kappa_{\rm ex,2}}\hat{\xi}_2\\
&\quad+\sqrt{\frac{\kappa_{\rm ex,3}}{2}}\hat{\xi}_3-\sqrt{\frac{\kappa_{\rm ex,4}}{2}}\hat{\xi}_4,\\
\frac{d\delta\hat{b}}{dt} &= \Big[-i\omega_{\rm b}-\frac{\gamma_{\rm m}}{2}\Big]\delta\hat{b}-iG^*(\delta\hat{a}_1+\delta\hat{a}_2)-\sqrt{\gamma_{\rm m}}\hat{b}_{\rm in},
\end{aligned} \tag{B4}$$

where $G=g_{\rm om}(\alpha_1+\alpha_2)/2$. The steady-state solutions of α_1 and α_2 can be obtained from Eq. (B3) as

$$\begin{aligned}
\alpha_1 &= \frac{\sqrt{\kappa_{\rm ex,1}}[i(\Delta'-\delta_{\rm s})+\kappa_2]\alpha_{\rm in,1}-\sqrt{\kappa_{\rm ex,2}}g'\alpha_{\rm in,2}}{-[i(\Delta'+\delta_{\rm s})+\kappa_1][i(\Delta'-\delta_{\rm s})+\kappa_2]+g'^2},\\
\alpha_2 &= \frac{\sqrt{\kappa_{\rm ex,2}}[i(\Delta'+\delta_{\rm s})+\kappa_1]\alpha_{\rm in,2}-\sqrt{\kappa_{\rm ex,1}}g'\alpha_{\rm in,1}}{-[i(\Delta'+\delta_{\rm s})+\kappa_1][i(\Delta'-\delta_{\rm s})+\kappa_2]+g'^2},\\
\alpha_{\rm b} &= \frac{-i\frac{g_{\rm om}}{2}(|\alpha_1|^2+|\alpha_2|^2+\alpha_1^*\alpha_2+\alpha_2^*\alpha_1)}{i\omega_{\rm b}+\frac{\gamma_{\rm m}}{2}}.
\end{aligned} \tag{B5}$$

The fluctuation operators are correspondingly expressed as

$$\begin{aligned}
\delta\hat{a}_1 &= f_{1,1}\hat{\xi}_{\rm ex,1}+f_{1,2}\hat{\xi}_{\rm ex,2}+f_{1,3}\hat{\xi}_3+f_{1,4}\hat{\xi}_4\\
&\quad+f_{1,\rm A}\hat{\xi}_{\rm A}+f_{1,\rm B}\hat{\xi}_{\rm B}+f_{1,\rm b}\hat{b}_{\rm in},\\
\delta\hat{a}_2 &= f_{2,1}\hat{\xi}_{\rm ex,1}+f_{2,2}\hat{\xi}_{\rm ex,2}+f_{2,3}\hat{\xi}_3+f_{2,4}\hat{\xi}_4\\
&\quad+f_{2,\rm A}\hat{\xi}_{\rm A}+f_{2,\rm B}\hat{\xi}_{\rm B}+f_{2,\rm b}\hat{b}_{\rm in},\\
\delta\hat{b} &= f_{\rm b,1}\hat{\xi}_{\rm ex,1}+f_{\rm b,2}\hat{\xi}_{\rm ex,2}+f_{\rm b,3}\hat{\xi}_3+f_{\rm b,4}\hat{\xi}_4\\
&\quad+f_{\rm b,A}\hat{\xi}_{\rm A}+f_{\rm b,B}\hat{\xi}_{\rm B}+f_{\rm b,b}\hat{b}_{\rm in},
\end{aligned} \tag{B6}$$

where

$$\begin{aligned}
f_{1,1} &= \frac{|G|^2\sqrt{\kappa_{\rm ex,1}}+\big(i\omega_{\rm b}+\frac{\gamma_{\rm m}}{2}\big)[i(\Delta'-\delta_{\rm s})+\kappa_2]\sqrt{\kappa_{\rm ex,1}}}{2g'|G|^2-|G|^2(2i\Delta'+\kappa_1+\kappa_2)+g'^2\big(i\omega_{\rm b}+\frac{\gamma_{\rm m}}{2}\big)-[i(\Delta'+\delta_{\rm s})+\kappa_1][i(\Delta'-\delta_{\rm s})+\kappa_2]\big(i\omega_{\rm b}+\frac{\gamma_{\rm m}}{2}\big)},\\
f_{1,2} &= \frac{|G|^2\sqrt{\kappa_{\rm ex,2}}-\big(i\omega_{\rm b}+\frac{\gamma_{\rm m}}{2}\big)g'\sqrt{\kappa_{\rm ex,2}}}{2g'|G|^2-|G|^2(2i\Delta'+\kappa_1+\kappa_2)+g'^2\big(i\omega_{\rm b}+\frac{\gamma_{\rm m}}{2}\big)-[i(\Delta'+\delta_{\rm s})+\kappa_1][i(\Delta'-\delta_{\rm s})+\kappa_2]\big(i\omega_{\rm b}+\frac{\gamma_{\rm m}}{2}\big)},\\
f_{1,3} &= \frac{|G|^2\sqrt{2\kappa_{\rm ex,3}}+\big(i\omega_{\rm b}+\frac{\gamma_{\rm m}}{2}\big)\sqrt{\frac{\kappa_{\rm ex,3}}{2}}[i(\Delta'-\delta_{\rm s})+\kappa_2+g']}{2g'|G|^2-|G|^2(2i\Delta'+\kappa_1+\kappa_2)+g'^2\big(i\omega_{\rm b}+\frac{\gamma_{\rm m}}{2}\big)-[i(\Delta'+\delta_{\rm s})+\kappa_1][i(\Delta'-\delta_{\rm s})+\kappa_2]\big(i\omega_{\rm b}+\frac{\gamma_{\rm m}}{2}\big)},\\
f_{1,4} &= \frac{\sqrt{\frac{\kappa_{\rm ex,4}}{2}}\big(i\omega_{\rm b}+\frac{\gamma_{\rm m}}{2}\big)[i(\Delta'-\delta_{\rm s})+\kappa_2-g']}{2g'|G|^2-|G|^2(2i\Delta'+\kappa_1+\kappa_2)+g'^2\big(i\omega_{\rm b}+\frac{\gamma_{\rm m}}{2}\big)-[i(\Delta'+\delta_{\rm s})+\kappa_1][i(\Delta'-\delta_{\rm s})+\kappa_2]\big(i\omega_{\rm b}+\frac{\gamma_{\rm m}}{2}\big)},\\
f_{1,\rm b} &= \frac{-i\sqrt{\gamma_{\rm m}}G[i(\Delta'-\delta_{\rm s})+\kappa_2-g']}{2g'|G|^2-|G|^2(2i\Delta'+\kappa_1+\kappa_2)+g'^2\big(i\omega_{\rm b}+\frac{\gamma_{\rm m}}{2}\big)-[i(\Delta'+\delta_{\rm s})+\kappa_1][i(\Delta'-\delta_{\rm s})+\kappa_2]\big(i\omega_{\rm b}+\frac{\gamma_{\rm m}}{2}\big)},\\
f_{1,\rm A} &= f_{1,1}\cos\theta-if_{1,2}e^{-i\varphi}\sin\theta,\quad f_{1,\rm B}=f_{1,2}\cos\theta-if_{1,1}e^{i\varphi}\sin\theta,
\end{aligned} \tag{B7}$$

$$\begin{aligned}
f_{2,1} &= \frac{-|G|^2\sqrt{\kappa_{\rm ex,1}}-\big(i\omega_{\rm b}+\frac{\gamma_{\rm m}}{2}\big)g'\sqrt{\kappa_{\rm ex,1}}}{2g'|G|^2-|G|^2(2i\Delta'+\kappa_1+\kappa_2)+g'^2\big(i\omega_{\rm b}+\frac{\gamma_{\rm m}}{2}\big)-[i(\Delta'+\delta_{\rm s})+\kappa_1][i(\Delta'-\delta_{\rm s})+\kappa_2]\big(i\omega_{\rm b}+\frac{\gamma_{\rm m}}{2}\big)},\\
f_{2,2} &= \frac{|G|^2\sqrt{\kappa_{\rm ex,2}}+\big(i\omega_{\rm b}+\frac{\gamma_{\rm m}}{2}\big)[i(\Delta'+\delta_{\rm s})+\kappa_1]\sqrt{\kappa_{\rm ex,2}}}{2g'|G|^2-|G|^2(2i\Delta'+\kappa_1+\kappa_2)+g'^2\big(i\omega_{\rm b}+\frac{\gamma_{\rm m}}{2}\big)-[i(\Delta'+\delta_{\rm s})+\kappa_1][i(\Delta'-\delta_{\rm s})+\kappa_2]\big(i\omega_{\rm b}+\frac{\gamma_{\rm m}}{2}\big)},\\
f_{2,3} &= \frac{-|G|^2\sqrt{2\kappa_{\rm ex,3}}-\big(i\omega_{\rm b}+\frac{\gamma_{\rm m}}{2}\big)\sqrt{\frac{\kappa_{\rm ex,3}}{2}}[i(\Delta'+\delta_{\rm s})+\kappa_1+g']}{2g'|G|^2-|G|^2(2i\Delta'+\kappa_1+\kappa_2)+g'^2\big(i\omega_{\rm b}+\frac{\gamma_{\rm m}}{2}\big)-[i(\Delta'+\delta_{\rm s})+\kappa_1][i(\Delta'-\delta_{\rm s})+\kappa_2]\big(i\omega_{\rm b}+\frac{\gamma_{\rm m}}{2}\big)},\\
f_{2,4} &= \frac{\sqrt{\frac{\kappa_{\rm ex,4}}{2}}\big(i\omega_{\rm b}+\frac{\gamma_{\rm m}}{2}\big)[i(\Delta'+\delta_{\rm s})+\kappa_1-g']}{2g'|G|^2-|G|^2(2i\Delta'+\kappa_1+\kappa_2)+g'^2\big(i\omega_{\rm b}+\frac{\gamma_{\rm m}}{2}\big)-[i(\Delta'+\delta_{\rm s})+\kappa_1][i(\Delta'-\delta_{\rm s})+\kappa_2]\big(i\omega_{\rm b}+\frac{\gamma_{\rm m}}{2}\big)},\\
f_{2,\rm b} &= \frac{-i\sqrt{\gamma_{\rm m}}G[i(\Delta'+\delta_{\rm s})+\kappa_1-g']}{2g'|G|^2-|G|^2(2i\Delta'+\kappa_1+\kappa_2)+g'^2\big(i\omega_{\rm b}+\frac{\gamma_{\rm m}}{2}\big)-[i(\Delta'+\delta_{\rm s})+\kappa_1][i(\Delta'-\delta_{\rm s})+\kappa_2]\big(i\omega_{\rm b}+\frac{\gamma_{\rm m}}{2}\big)},\\
f_{2,\rm A} &= f_{2,1}\cos\theta-if_{2,2}e^{-i\varphi}\sin\theta,\quad f_{2,\rm B}=f_{2,2}\cos\theta-if_{2,1}e^{i\varphi}\sin\theta,
\end{aligned} \tag{B8}$$

and

$$
\begin{aligned}
f_{\mathrm{b},1} &= \frac{ig'G^*\sqrt{\kappa_{\mathrm{ex},1}} - iG^*[i(\Delta'-\delta_\mathrm{s})+\kappa_2]\sqrt{\kappa_{\mathrm{ex},1}}}{2g'|G|^2 - |G|^2(2i\Delta'+\kappa_1+\kappa_2) + g'^2\left(i\omega_\mathrm{b}+\frac{\gamma_\mathrm{m}}{2}\right) - [i(\Delta'+\delta_\mathrm{s})+\kappa_1][i(\Delta'-\delta_\mathrm{s})+\kappa_2]\left(i\omega_\mathrm{b}+\frac{\gamma_\mathrm{m}}{2}\right)},\\
f_{\mathrm{b},2} &= \frac{ig'G^*\sqrt{\kappa_{\mathrm{ex},2}} - iG^*[i(\Delta'+\delta_\mathrm{s})+\kappa_1]\sqrt{\kappa_{\mathrm{ex},2}}}{2g'|G|^2 - |G|^2(2i\Delta'+\kappa_1+\kappa_2) + g'^2\left(i\omega_\mathrm{b}+\frac{\gamma_\mathrm{m}}{2}\right) - [i(\Delta'+\delta_\mathrm{s})+\kappa_1][i(\Delta'-\delta_\mathrm{s})+\kappa_2]\left(i\omega_\mathrm{b}+\frac{\gamma_\mathrm{m}}{2}\right)},\\
f_{\mathrm{b},3} &= \frac{-iG^*\sqrt{\frac{\kappa_{\mathrm{ex},3}}{2}}(-2i\delta_\mathrm{s}+\kappa_2-\kappa_1)}{2g'|G|^2 - |G|^2(2i\Delta'+\kappa_1+\kappa_2) + g'^2\left(i\omega_\mathrm{b}+\frac{\gamma_\mathrm{m}}{2}\right) - [i(\Delta'+\delta_\mathrm{s})+\kappa_1][i(\Delta'-\delta_\mathrm{s})+\kappa_2]\left(i\omega_\mathrm{b}+\frac{\gamma_\mathrm{m}}{2}\right)},\\
f_{\mathrm{b},4} &= \frac{ig'G^*\sqrt{2\kappa_{\mathrm{ex},4}} - iG^*\sqrt{\frac{\kappa_{\mathrm{ex},4}}{2}}(2i\Delta'+\kappa_2+\kappa_1)}{2g'|G|^2 - |G|^2(2i\Delta'+\kappa_1+\kappa_2) + g'^2\left(i\omega_\mathrm{b}+\frac{\gamma_\mathrm{m}}{2}\right) - [i(\Delta'+\delta_\mathrm{s})+\kappa_1][i(\Delta'-\delta_\mathrm{s})+\kappa_2]\left(i\omega_\mathrm{b}+\frac{\gamma_\mathrm{m}}{2}\right)},\\
f_{\mathrm{b,b}} &= \frac{\sqrt{\gamma_\mathrm{m}}\{[i(\Delta'+\delta_\mathrm{s})+\kappa_1][i(\Delta'-\delta_\mathrm{s})+\kappa_2]-g'^2\}}{2g'|G|^2 - |G|^2(2i\Delta'+\kappa_1+\kappa_2) + g'^2\left(i\omega_\mathrm{b}+\frac{\gamma_\mathrm{m}}{2}\right) - [i(\Delta'+\delta_\mathrm{s})+\kappa_1][i(\Delta'-\delta_\mathrm{s})+\kappa_2]\left(i\omega_\mathrm{b}+\frac{\gamma_\mathrm{m}}{2}\right)},\\
f_{\mathrm{b,A}} &= f_{\mathrm{b},1}\cos\theta - if_{\mathrm{b},2}e^{-i\varphi}\sin\theta,\\
f_{\mathrm{b,B}} &= f_{\mathrm{b},2}\cos\theta - if_{\mathrm{b},1}e^{i\varphi}\sin\theta.
\end{aligned}
\tag{B9}
$$

By setting $\theta=\pi/2$, the steady-state output field $\hat{d}_\mathrm{b}$ can be obtained from the cavity input-output relations as

$$
\begin{aligned}
\hat{d}_\mathrm{b} = {} & F_0 + F_1\hat{\xi}_1 + F_2\hat{\xi}_2 + F_3\hat{\xi}_3 + F_4\hat{\xi}_4\\
& + F_5\hat{\xi}_\mathrm{A} + F_6\hat{\xi}_\mathrm{B} + F_\mathrm{b}\hat{b}_\mathrm{in},
\end{aligned}
\tag{B10}
$$

where

$$
\begin{aligned}
F_0 &= -ie^{-i\varphi}\alpha + \sqrt{\frac{\kappa_{\mathrm{ex},2}}{2}}\alpha_2 - ie^{-i\varphi}\sqrt{\frac{\kappa_{\mathrm{ex},1}}{2}}\alpha_1,\\
F_1 &= \sqrt{\frac{\kappa_{\mathrm{ex},2}}{2}}f_{2,1} - \frac{ie^{-i\varphi}}{\sqrt{2}}(1+\sqrt{\kappa_{\mathrm{ex},1}}f_{1,1}),\\
F_2 &= \frac{1}{\sqrt{2}}(1+\sqrt{\kappa_{\mathrm{ex},2}}f_{2,2}) - ie^{-i\varphi}\sqrt{\frac{\kappa_{\mathrm{ex},1}}{2}}f_{1,2},\\
F_3 &= \sqrt{\frac{\kappa_{\mathrm{ex},2}}{2}}f_{2,3} - ie^{-i\varphi}\sqrt{\frac{\kappa_{\mathrm{ex},1}}{2}}f_{1,3},\\
F_4 &= \sqrt{\frac{\kappa_{\mathrm{ex},2}}{2}}f_{2,4} - ie^{-i\varphi}\sqrt{\frac{\kappa_{\mathrm{ex},1}}{2}}f_{1,4},\\
F_5 &= -ie^{-i\varphi} + \sqrt{\frac{\kappa_{\mathrm{ex},2}}{2}}f_{2,\mathrm{A}} - ie^{-i\varphi}\sqrt{\frac{\kappa_{\mathrm{ex},1}}{2}}f_{1,\mathrm{A}}\\
F_6 &= \sqrt{\frac{\kappa_{\mathrm{ex},2}}{2}}f_{2,\mathrm{B}} - ie^{-i\varphi}\sqrt{\frac{\kappa_{\mathrm{ex},1}}{2}}f_{1,\mathrm{B}},\\
F_\mathrm{b} &= \sqrt{\frac{\kappa_{\mathrm{ex},2}}{2}}f_{2,5} - ie^{-i\varphi}\sqrt{\frac{\kappa_{\mathrm{ex},1}}{2}}f_{1,5}.
\end{aligned}
\tag{B11}
$$

In the absence of quantum and thermal noise, the transmission spectrum of the NHMI reads

$$
T = \frac{\langle\hat{d}_\mathrm{b}^\dagger\hat{d}_\mathrm{b}\rangle}{|\alpha|^2} = |F_0|^2. \tag{B12}
$$

For the HMI, the Langevin equations can be obtained from Eqs. (A2) and (A5),

$$
\begin{aligned}
\frac{d\hat{b}'}{dt} &= \left(-i\omega_\mathrm{b}-\frac{\gamma_\mathrm{m}}{2}\right)\hat{b}' - i\frac{g_\mathrm{om}}{2}(\hat{a}_1'^\dagger+\hat{a}_2'^\dagger)(\hat{a}_1'+\hat{a}_2') - \sqrt{\gamma_\mathrm{m}}\hat{b}_\mathrm{in},\\
\frac{d\hat{a}_1'}{dt} &= [-i\Delta'-\kappa_1']\hat{a}_1' - \sqrt{\kappa_{\mathrm{ex},1}'}(\alpha_{\mathrm{in},1}+\hat{\xi}_1) - \sqrt{\kappa_{\mathrm{ex},3}'}\hat{\xi}_3,\\
\frac{d\hat{a}_2'}{dt} &= [-i\Delta-\kappa_2']\hat{a}_2' - \sqrt{\kappa_{\mathrm{ex},2}'}(\alpha_{\mathrm{in},2}+\hat{\xi}_2) - \sqrt{\kappa_{\mathrm{ex},4}'}\hat{\xi}_4,
\end{aligned}
\tag{B13}
$$

where $\kappa_1'=(\kappa_{\mathrm{ex},1}'+\kappa_{\mathrm{ex},3}')/2$ and $\kappa_2'=(\kappa_{\mathrm{ex},2}'+\kappa_{\mathrm{ex},4}')/2$.

Similarly, following the procedure in Eqs. (B3) and (B4), we linearize cavity modes $\hat{a}_1'$ and $\hat{a}_2'$, as well as mechanical mode $\hat{b}'$, and obtain the steady-state solutions for the HMI,

$$
\begin{aligned}
\alpha_1' &= -\frac{\sqrt{\kappa_{\mathrm{ex},1}}\alpha_{\mathrm{in},1}}{i\Delta_1'+\kappa_1'},\\
\alpha_2' &= -\frac{\sqrt{\kappa_{\mathrm{ex},2}}\alpha_{\mathrm{in},2}}{i\Delta_2+\kappa_2'},\\
\alpha_\mathrm{b}' &= -\frac{ig_\mathrm{om}|\alpha_1|^2}{i\omega_\mathrm{b}+\frac{\gamma_\mathrm{m}}{2}},
\end{aligned}
\tag{B14}
$$

and the fluctuations for the HMI,

$$
\begin{aligned}
\delta\hat{a}_1' = {} & f_{1,1}'\hat{\xi}_1 + f_{1,2}'\hat{\xi}_2 + f_{1,3}'\hat{\xi}_3 + f_{1,4}'\hat{\xi}_4\\
& + f_{1,A}'\hat{\xi}_\mathrm{A} + f_{1,B}'\hat{\xi}_\mathrm{B} + f_{1,\mathrm{b}}'\hat{b}_\mathrm{in},\\
\delta\hat{a}_2' = {} & f_{2,1}'\hat{\xi}_1 + f_{2,2}'\hat{\xi}_2 + f_{2,3}'\hat{\xi}_3 + f_{2,4}'\hat{\xi}_4\\
& + f_{2,A}'\hat{\xi}_\mathrm{A} + f_{2,B}'\hat{\xi}_\mathrm{B} + f_{2,\mathrm{b}}'\hat{b}_\mathrm{in},\\
\delta\hat{b}' = {} & f_{\mathrm{b},1}'\hat{\xi}_1 + f_{\mathrm{b},2}'\hat{\xi}_2 + f_{\mathrm{b},3}'\hat{\xi}_3 + f_{\mathrm{b},4}'\hat{\xi}_4 + f_{b,A}'\hat{\xi}_\mathrm{A}\\
& + f_{b,B}'\hat{\xi}_\mathrm{B} + f_{\mathrm{b,b}}'\hat{b}_\mathrm{in},
\end{aligned}
\tag{B15}
$$

where

$$
\begin{aligned}
f'_{1,1} &= \frac{-\left(i\omega_{\rm b}+\frac{\gamma_{\rm m}}{2}\right)\sqrt{\kappa_{\rm ex,1}}}{[i(\Delta'+\delta_{\rm s})+\kappa_1]\left(i\omega_{\rm b}+\frac{\gamma_{\rm m}}{2}\right)+g_{\rm om}^2|\alpha'_1|^2},\\
f'_{1,2} &= f'_{1,4}=0,\\
f'_{1,3} &= \frac{-\left(i\omega_{\rm b}+\frac{\gamma_{\rm m}}{2}\right)\sqrt{\kappa_{\rm ex,3}}}{[i(\Delta'+\delta_{\rm s})+\kappa_1]\left(i\omega_{\rm b}+\frac{\gamma_{\rm m}}{2}\right)+g_{\rm om}^2|\alpha'_1|^2},\\
f'_{1,\rm b} &= \frac{\sqrt{\gamma_{\rm m}}ig_{\rm om}\alpha'_1}{[i(\Delta'+\delta_{\rm s})+\kappa_1]\left(i\omega_{\rm b}+\frac{\gamma_{\rm m}}{2}\right)+g_{\rm om}^2|\alpha'_1|^2},\\
f'_{1,\rm A} &= f'_{1,1}\cos\theta - if'_{1,2}e^{-i\varphi}\sin\theta,\\
f'_{1,\rm B} &= f'_{1,2}\cos\theta - if'_{1,1}e^{i\varphi}\sin\theta,
\end{aligned}
\tag{B16}
$$

and

$$
\begin{aligned}
f'_{2,1} &= f'_{2,3}=f'_{2,5}=0,\\
f'_{2,2} &= \frac{-\sqrt{\kappa_{\rm ex,2}}}{i\Delta+\kappa'_2},\\
f'_{2,4} &= \frac{-\sqrt{\kappa_{\rm ex,4}}}{i\Delta+\kappa'_2},\\
f'_{2,\rm A} &= f'_{2,1}\cos\theta - if'_{2,2}e^{-i\varphi}\sin\theta,\\
f'_{2,\rm B} &= f'_{2,2}\cos\theta - if'_{2,1}e^{i\varphi}\sin\theta.
\end{aligned}
\tag{B17}
$$

The output field $\hat{d}'_{\rm b}$ of the HMI can then be expressed as

$$
\begin{aligned}
\hat{d}'_{\rm b} = F'_0 &+ F'_1\hat{\xi}_1 + F'_2\hat{\xi}_2 + F'_3\hat{\xi}_3 + F'_4\hat{\xi}_4\\
&+ F'_5\hat{\xi}_{\rm A} + F'_6\hat{\xi}_{\rm B} + F'_{\rm b}\hat{b}_{\rm in},
\end{aligned}
\tag{B18}
$$

where the coefficient $F'_{\rm m}$ with ${\rm m}\in\{0,1,2,3,4,5,6,{\rm b}\}$ has the same definition as that of Eq. (B11).

APPENDIX C: THE QUANTUM FISHER INFORMATION OF THE NHMI AND THE HMI

To quantitatively characterize the metrological performance of the NHMI, we evaluate the QFI associated with the estimation of the signal parameter $\delta_{\rm s}$. The QFI provides a fundamental bound on the achievable precision via the quantum Cramér-Rao bound, ${\rm Var}(\delta_{\rm s})\geqslant 1/F_{\rm Q}(\delta_{\rm s})$.

In both the NHMI and the HMI, the probe field is prepared in a coherent state, and the system dynamics are linearized around the steady state. Consequently, the output field remains Gaussian, and the QFI can be efficiently evaluated within the amplitude vector $\boldsymbol{\mu}_{\rm out}$ and covariance matrix $\mathbf{V}_{\rm out}$ of the output field [98]. In the following, we present a unified derivation of the QFI applicable to both the NHMI and the HMI. We first introduce a pair of quadrature operators, conventionally referred to as the "position" and "momentum" operators, defined as

$$
\begin{aligned}
\hat{X}_{\rm b} &= \frac{\hat{d}_{\rm b}+\hat{d}_{\rm b}^\dagger}{\sqrt{2}},\\
\hat{Y}_{\rm b} &= \frac{\hat{d}_{\rm b}-\hat{d}_{\rm b}^\dagger}{\sqrt{2}}.
\end{aligned}
\tag{C1}
$$

The amplitude vector $\boldsymbol{\mu}_{\rm out}$ is given by

$$
\langle\boldsymbol{\mu}_{\rm out}\rangle = \begin{bmatrix}\langle\hat{X}_{\rm b}\rangle\\ \langle\hat{Y}_{\rm b}\rangle\end{bmatrix} = \begin{bmatrix}\sqrt{2}{\rm Re}[F_0]\\ \sqrt{2}{\rm Im}[F_0]\end{bmatrix}. \tag{C2}
$$

According to the definition of elements of the covariance matrix $V_{\rm j,k}=1/2\langle\hat{x}_{\rm j}\hat{x}_{\rm k}+\hat{x}_{\rm k}\hat{x}_{\rm j}\rangle-\langle\hat{x}_{\rm j}\rangle\langle\hat{x}_{\rm k}\rangle$, with $j(\hat{k})\in\{\hat{X}_{\rm b},\hat{Y}_{\rm b}\}$. We can obtain the covariance matrix $\mathbf{V}_{\rm out}$,

$$
\mathbf{V}_{\rm out} = \begin{bmatrix}\frac{\sum_{i=1}^{6}|F_i|^2+|F_{\rm b}|^2(2n_{\rm th}+1)}{4} & 0\\ 0 & \frac{\sum_{i=1}^{6}|F_i|^2+|F_{\rm b}|^2(2n_{\rm th}+1)}{4}\end{bmatrix}. \tag{C3}
$$

The QFI for the NHMI is then given by

$$
\begin{aligned}
F_{\rm Q} &= \left(\frac{d\boldsymbol{\mu}_{\rm out}}{d\delta_{\rm s}}\right)^T\mathbf{V}_{\rm out}^{-1}\left(\frac{{\rm d}\boldsymbol{\mu}_{\rm out}}{{\rm d}\delta_{\rm s}}\right)\\
&= \frac{2}{\sum_{n=1}^{6}|F_{\rm n}|^2+|F_{\rm b}|^2(2n_{\rm th}+1)}\left|\frac{dF_0}{d\delta_{\rm s}}\right|^2.
\end{aligned}
\tag{C4}
$$

For the HMI, the corresponding QFI is obtained by replacing $F_{\rm i}$ with $F'_{\rm i}$.

To quantify the enhancement in metrological performance, we define the enhancement factor $E_{\rm F}=F_{\rm Q}^{\rm NHMI}/F_{\rm Q}^{\rm HMI}$, as shown in Fig. 6. It decreases from a large value at a small $\delta_{\rm s}$ to a vanishing value as $\delta_{\rm s}$ increases. The QFI enhancement is large before the EP, $\delta_{\rm s}<0.05\kappa_{\rm ex}$. The nonzero QFI appears because the total QFI of the system is calculated and the imaginary parts of the eigenvalues split, similar to Ref. [100]. However, it is difficult to determine the loss difference of the eigenvectors. Here, we are interested in the real parts of the eigenvalues after the EP. When biased after EP, the eigenfrequencies split and the QFI is still greatly enhanced in comparison with the HMI.

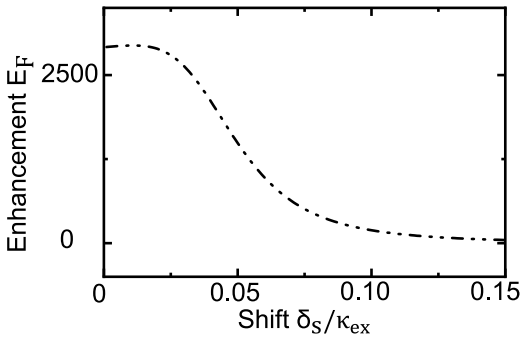


FIG. 6. QFI enhancement $E_{\rm F}$ as a function of $\delta_{\rm s}$. The parameters are set as $\theta=\pi/4$, $\varphi=\pi/2$, $\Delta=0$, $\omega_{\rm b}=0.1\kappa_{\rm ex}$, $\gamma_{\rm m}=10^{-4}\kappa_{\rm ex}$, $n_{\rm th}=10^7$, $\kappa_{\rm ex,3}=0.2\kappa_{\rm ex}$, and $\kappa_{\rm ex,4}=0$.

[1] A. A. Michelson and E. W. Morley, On the relative motion of the Earth and the Luminiferous Ether, Am. J. Sci. **s3-34**, 333 (1887).

[2] A. Abramovici, W. E. Althouse, R. W. P. Drever, Y. Gürsel, S. Kawamura, F. J. Raab, D. Shoemaker, L. Sievers, R. E. Spero, K. S. Thorne, R. E. Vogt, R. Weiss, S. E. Whitcomb, and M. E. Zucker, LIGO: The laser interferometer gravitational-wave observatory, Science **256**, 325 (1992).

[3] B. P. Abbott, R. Abbott, R. Adhikari, P. Ajith, B. Allen, G. Allen, R. S. Amin, S. B. Anderson, W. G. Anderson, M. A. Arain, M. Araya, H. Armandula, P. Armor, Y. Aso, S. Aston, P. Aufmuth, C. Aulbert, S. Babak, P. Baker, S. Ballmer, *et al.*, LIGO: The laser interferometer gravitational-wave observatory, Rep. Prog. Phys. **72**, 076901 (2009).

[4] M. Tse, H. Yu, N. Kijbunchoo, A. Fernandez-Galiana, P. Dupej, L. Barsotti, C. D. Blair, D. D. Brown, S. E. Dwyer, A. Effler, M. Evans, P. Fritschel, V. V. Frolov, A. C. Green, G. L. Mansell, F. Matichard, N. Mavalvala, D. E. McClelland, L. McCuller, T. McRae, *et al.*, Quantum-enhanced advanced LIGO detectors in the era of gravitational-wave astronomy, Phys. Rev. Lett. **123**, 231107 (2019).

[5] A. Buikema, C. Cahillane, G. L. Mansell, C. D. Blair, R. Abbott, C. Adams, R. X. Adhikari, A. Ananyeva, S. Appert, K. Arai, J. S. Areeda, Y. Asali, S. M. Aston, C. Austin, A. M. Baer, M. Ball, S. W. Ballmer, S. Banagiri, D. Barker, L. Barsotti, *et al.*, Sensitivity and performance of the advanced LIGO detectors in the third observing run, Phys. Rev. D **102**, 062003 (2020).

[6] D. Ganapathy, W. Jia, M. Nakano, V. Xu, N. Aritomi, T. Cullen, N. Kijbunchoo, S. E. Dwyer, A. Mullavey, L. McCuller, R. Abbott, I. Abouelfettouh, R. X. Adhikari, A. Ananyeva, S. Appert, K. Arai, S. M. Aston, M. Ball, S. W. Ballmer, D. Barker, *et al.*, Broadband quantum enhancement of the LIGO detectors with frequency-dependent squeezing, Phys. Rev. X **13**, 041021 (2023).

[7] W. Jia, V. Xu, K. Kuns, M. Nakano, L. Barsotti, M. Evans, N. Mavalvala, R. Abbott, I. Abouelfettouh, R. X. Adhikari, A. Ananyeva, S. Appert, K. Arai, N. Aritomi, S. M. Aston, M. Ball, S. W. Ballmer, D. Barker, B. K. Berger, J. Betzwieser, *et al.*, Squeezing the quantum noise of a gravitational-wave detector below the standard quantum limit, Science **385**, 1318 (2024).

[8] K.-S. Isleif, G. Heinzel, M. Mehmet, and O. Gerberding, Compact multifringe interferometry with subpicometer precision, Phys. Rev. Appl. **12**, 034025 (2019).

[9] J. Smetana, R. Walters, S. Bauchinger, A. S. Ubhi, S. Cooper, D. Hoyland, R. Abbott, C. Baune, P. Fritchel, O. Gerberding, S. Köhnke, H. Miao, S. Rode, and D. Martynov, Compact Michelson interferometers with subpicometer sensitivity, Phys. Rev. Appl. **18**, 034040 (2022).

[10] Z. Tian, S. S.-H. Yam, and H.-P. Loock, Refractive index sensor based on an abrupt taper Michelson interferometer in a single-mode fiber, Opt. Lett. **33**, 1105 (2008).

[11] Z. Tian and S. S.-H. Yam, In-line single-mode optical fiber interferometric refractive index sensors, J. Lightwave Technol. **27**, 2296 (2009).

[12] Y. Zhao, M. Dai, Z. Chen, X. Liu, M. S. A. Gandhi, Q. Li, and H. Y. Fu, Ultrasensitive temperature sensor with Vernier-effect improved fiber Michelson interferometer, Opt. Express **29**, 1090 (2021).

[13] Y. Han, B. Liu, Y. Wu, Y. Mao, J. Wu, L. Zhao, T. Nan, J. Wang, R. Tang, Y. Zhang, and Y. Liu, Ultra-compact silicon-microcap based improved Michelson interferometer high-temperature sensor, Opt. Express **29**, 6703 (2021).

[14] A. Xuereb, R. Schnabel, and K. Hammerer, Dissipative optomechanics in a Michelson-Sagnac interferometer, Phys. Rev. Lett. **107**, 213604 (2011).

[15] A. Sawadsky, H. Kaufer, R. M. Nia, S. P. Tarabrin, F. Y. Khalili, K. Hammerer, and R. Schnabel, Observation of generalized optomechanical coupling and cooling on cavity resonance, Phys. Rev. Lett. **114**, 043601 (2015).

[16] F. Y. Khalili, S. P. Tarabrin, K. Hammerer, and R. Schnabel, Generalized analysis of quantum noise and dynamic backaction in signal-recycled Michelson-type laser interferometers, Phys. Rev. A **94**, 013844 (2016).

[17] C. Bond, D. Brown, A. Freise, and K. A. Strain, Interferometer techniques for gravitational-wave detection, Living. Rev. Relativ. **19**, 3 (2016).

[18] G. Marra, C. Clivati, R. Luckett, A. Tampellini, J. Kronjäger, L. Wright, A. Mura, F. Levi, S. Robinson, A. Xuereb, B. Baptie, and D. Calonico, Ultrastable laser interferometry for earthquake detection with terrestrial and submarine cables, Science **361**, 486 (2018).

[19] M. Chwalla, K. Danzmann, M. Dovale Álvarez, J. J. Esteban Delgado, G. Fernández Barranco, E. Fitzsimons, O. Gerberding, G. Heinzel, C. J. Killow, M. Lieser, M. Perreur-Lloyd, D. I. Robertson, J. M. Rohr, S. Schuster, T. S. Schwarze, M. Tröbs, G. Wanner, and H. Ward, Optical suppression of tilt-to-length coupling in the LISA long-arm interferometer, Phys. Rev. Appl. **14**, 014030 (2020).

[20] A. Buonanno and Y. Chen, Quantum noise in second generation, signal-recycled laser interferometric gravitational-wave detectors, Phys. Rev. D **64**, 042006 (2001).

[21] K. Goda, O. Miyakawa, E. E. Mikhailov, S. Saraf, R. Adhikari, K. McKenzie, R. Ward, S. Vass, A. J. Weinstein, and N. Mavalvala, A quantum-enhanced prototype gravitational-wave detector, Nat. Phys. **4**, 472 (2008).

[22] J. Lough, E. Schreiber, F. Bergamin, H. Grote, M. Mehmet, H. Vahlbruch, C. Affeldt, M. Brinkmann, A. Bisht, V. Kringel, H. Lück, N. Mukund, S. Nadji, B. Sorazu, K. Strain, M. Weinert, and K. Danzmann, First demonstration of 6 dB quantum noise reduction in a kilometer scale gravitational wave observatory, Phys. Rev. Lett. **126**, 041102 (2021).

[23] J. Heinze, K. Danzmann, B. Willke, and H. Vahlbruch, 10 dB quantum-enhanced Michelson interferometer with balanced homodyne detection, Phys. Rev. Lett. **129**, 031101 (2022).

[24] N. Kalinin, T. Dirmeier, A. A. Sorokin, E. A. Anashkina, L. L. Sánchez-Soto, J. F. Corney, G. Leuchs, and A. V. Andrianov, Quantum-enhanced interferometer using Kerr squeezing, Nanophotonics **12**, 2945 (2023).

[25] P. R. Saulson, Thermal noise in mechanical experiments, Phys. Rev. D **42**, 2437 (1990).

[26] Y. Levin, Internal thermal noise in the LIGO test masses: A direct approach, Phys. Rev. D **57**, 659 (1998).

[27] C. Panuski, D. Englund, and R. Hamerly, Fundamental thermal noise limits for optical microcavities, Phys. Rev. X **10**, 041046 (2020).

[28] G. M. Harry, A. M. Gretarsson, P. R. Saulson, S. E. Kittelberger, S. D. Penn, W. J. Startin, S. Rowan, M. M. Fejer, D. R. M. Crooks, G. Cagnoli, J. Hough, and N. Nakagawa,

Thermal noise in interferometric gravitational wave detectors due to dielectric optical coatings, Class. Quantum Grav. **19**, 897 (2002).

[29] K. Numata, A. Kemery, and J. Camp, Thermal-noise limit in the frequency stabilization of lasers with rigid cavities, Phys. Rev. Lett. **93**, 250602 (2004).

[30] E. Capote, W. Jia, N. Aritomi, M. Nakano, V. Xu, R. Abbott, I. Abouelfettouh, R. X. Adhikari, A. Ananyeva, S. Appert, S. K. Apple, K. Arai, S. M. Aston, M. Ball, S. W. Ballmer, D. Barker, L. Barsotti, B. K. Berger, J. Betzwieser, D. Bhattacharjee, *et al.*, Advanced LIGO detector performance in the fourth observing run, Phys. Rev. D **111**, 062002 (2025).

[31] C. Whittle, L. McCuller, V. Sudhir, and M. Evans, Unification of thermal and quantum noises in gravitational-wave detectors, Phys. Rev. Lett. **130**, 241401 (2023).

[32] S. Gras, H. Yu, W. Yam, D. Martynov, and M. Evans, Audio-band coating thermal noise measurement for advanced LIGO with a multimode optical resonator, Phys. Rev. D **95**, 022001 (2017).

[33] G. I. McGhee, V. Spagnuolo, N. Demos, S. C. Tait, P. G. Murray, M. Chicoine, P. Dabadie, S. Gras, J. Hough, G. A. Iandolo, R. Johnston, V. Martinez, O. Patane, S. Rowan, F. Schiettekatte, J. R. Smith, L. Terkowski, L. Zhang, M. Evans, I. W. Martin, *et al.*, Titania mixed with silica: A low thermal-noise coating material for gravitational-wave detectors, Phys. Rev. Lett. **131**, 171401 (2023).

[34] T. Akutsu, M. Ando, K. Arai, Y. Arai, S. Araki, A. Araya, N. Aritomi, H. Asada, Y. Aso, S. Atsuta, K. Awai, S. Bae, L. Baiotti, M. A. Barton, K. Cannon, E. Capocasa, C.-S. Chen, T.-W. Chiu, K. Cho, Y.-K. Chu, *et al.*, KAGRA: 2.5 generation interferometric gravitational wave detector, Nat. Astron. **3**, 35 (2019).

[35] L. Hu, N. Poli, L. Salvi, and G. M. Tino, Atom interferometry with the Sr optical clock transition, Phys. Rev. Lett. **119**, 263601 (2017).

[36] M. Chiarotti, J. N. Tinsley, S. Bandarupally, S. Manzoor, M. Sacco, L. Salvi, and N. Poli, Practical limits for large-momentum-transfer clock atom interferometers, PRX Quantum **3**, 030348 (2022).

[37] J. S. Higgins, T. Ooi, J. F. Doyle, C. Zhang, J. Ye, K. Beeks, T. Sikorsky, and T. Schumm, Temperature sensitivity of a Thorium-229 solid-state nuclear clock, Phys. Rev. Lett. **134**, 113801 (2025).

[38] J. C. Saywell, M. S. Carey, P. S. Light, S. S. Szigeti, A. R. Milne, K. S. Gill, M. L. Goh, V. S. Perunicic, N. M. Wilson, C. D. Macrae, A. Rischka, P. J. Everitt, N. P. Robins, R. P. Anderson, M. R. Hush, and M. J. Biercuk, Enhancing the sensitivity of atom-interferometric inertial sensors using robust control, Nat. Commun. **14**, 7626 (2023).

[39] Y. Leng, Y. Chen, R. Li, L. Wang, H. Wang, L. Wang, H. Xie, C.-K. Duan, P. Huang, and J. Du, Measurement of the earth tides with a diamagnetic-levitated micro-oscillator at room temperature, Phys. Rev. Lett. **132**, 123601 (2024).

[40] J. Qian, J. Li, S.-Y. Zhu, J. You, and Y.-P. Wang, Probing PT-symmetry breaking of non-Hermitian topological photonic states via strong photon-magnon coupling, Phys. Rev. Lett. **132**, 156901 (2024).

[41] R. Ye, Y. He, G. Li, L. Wang, X. Wu, X. Qiao, Y. Zheng, L. Jin, D.-W. Wang, L. Yuan, and X. Chen, Observing non-Hermiticity induced chirality breaking in a synthetic Hall ladder, Light: Sci. Appl. **14**, 39 (2025).

[42] H. Qi, Y. Li, X. Wang, Y. Li, X. Li, X. Wang, X. Hu, and Q. Gong, Dynamically encircling exceptional points in different Riemann sheets for orbital angular momentum topological charge conversion, Phys. Rev. Lett. **132**, 243802 (2024).

[43] T. Dai, Y. Ao, J. Mao, Y. Yang, Y. Zheng, C. Zhai, Y. Li, J. Yuan, B. Tang, Z. Li, J. Luo, W. Wang, X. Hu, Q. Gong, and J. Wang, Non-Hermitian topological phase transitions controlled by nonlinearity, Nat. Phys. **20**, 101 (2024).

[44] Y.-K. Lu, P. Peng, Q.-T. Cao, D. Xu, J. Wiersig, Q. Gong, and Y.-F. Xiao, Spontaneous T-symmetry breaking and exceptional points in cavity quantum electrodynamics systems, Sci. Bull. **63**, 1096 (2018).

[45] W. Liu, Y. Wu, C.-K. Duan, X. Rong, and J. Du, Dynamically encircling an exceptional point in a real quantum system, Phys. Rev. Lett. **126**, 170506 (2021).

[46] Y. Wang, Y. Wu, X. Ye, C.-K. Duan, Y. Wang, H. Hu, X. Rong, and J. Du, Non-Hermitian non-Abelian topological transition in the $S = 1$ electron spin system of a nitrogen vacancy centre in diamond, Nat. Nanotechnol. **20**, 873 (2025).

[47] Y. Wu, Y. Wang, X. Ye, W. Liu, Z. Niu, C.-K. Duan, Y. Wang, X. Rong, and J. Du, Third-order exceptional line in a nitrogen-vacancy spin system, Nat. Nanotechnol. **19**, 160 (2024).

[48] M. Yang, Y.-W. Liao, H.-Q. Zhang, Y. Li, Z.-H. Hao, Z.-W. Zhou, X.-W. Luo, J.-S. Xu, C.-F. Li, and G.-C. Guo, Observing half-integer topological winding numbers in non-Hermitian synthetic lattices, Light: Sci. Appl. **14**, 225 (2025).

[49] Y. Li and Y.-C. Liu, Quantum signatures of the topological phase in bosonic quadratic systems, Phys. Rev. A **108**, 062405 (2023).

[50] X. Zhao, J. Wang, W. Liu, L. Shi, and J. Zi, Magnetically induced topological evolutions of exceptional points in photonic bands, Phys. Rev. Lett. **135**, 046203 (2025).

[51] Q.-B. Zeng, B. Zhu, S. Chen, L. You, and R. Lü, Non-Hermitian Kitaev chain with complex on-site potentials, Phys. Rev. A **94**, 022119 (2016).

[52] T. Liu, Y.-R. Zhang, Q. Ai, Z. Gong, K. Kawabata, M. Ueda, and F. Nori, Second-order topological phases in non-Hermitian systems, Phys. Rev. Lett. **122**, 076801 (2019).

[53] F. Di, W. Zhang, and X. Zhang, Observation of non-Hermitian topological synchronization, Commun. Phys. **8**, 78 (2025).

[54] Y. Li, C. Lu, S. Zhang, and Y.-C. Liu, Loss-induced Floquet non-Hermitian skin effect, Phys. Rev. B **108**, L220301 (2023).

[55] X. Huang, Y. Li, G.-F. Zhang, and Y.-C. Liu, Non-Hermitian skin effect and nonreciprocity induced by dissipative couplings, Phys. Rev. A **109**, L021503 (2024).

[56] G. Xu, X. Zhou, Y. Li, Q. Cao, W. Chen, Y. Xiao, L. Yang, and C.-W. Qiu, Non-Hermitian chiral heat transport, Phys. Rev. Lett. **130**, 266303 (2023).

[57] T. Wu, W. Zhang, H. Zhang, S. Hou, G. Chen, R. Liu, C. Lu, J. Li, R. Wang, P. Duan, J. Li, B. Wang, L. Shi, J. Zi, and X. Zhang, Vector exceptional points with strong superchiral fields, Phys. Rev. Lett. **124**, 083901 (2020).

[58] K. Liao, Y. Zhong, Z. Du, G. Liu, C. Li, X. Wu, C. Deng, C. Lu, X. Wang, C. T. Chan, Q. Song, S. Wang, X. Liu, X. Hu, and Q. Gong, On-chip integrated exceptional surface microlaser, Sci. Adv. **9**, eadf3470 (2023).

[59] J. Wiersig, Enhancing the sensitivity of frequency and energy splitting detection by using exceptional points: Application to

microcavity sensors for single-particle detection, Phys. Rev. Lett. **112**, 203901 (2014).
[60] C. Liang, Y. Tang, A.-N. Xu, and Y.-C. Liu, Observation of exceptional points in thermal atomic ensembles, Phys. Rev. Lett. **130**, 263601 (2023).
[61] Y.-T. Wang, Z.-A. Wang, Z.-P. Li, X.-D. Zeng, J.-M. Ren, W. Liu, Y.-Z. Yang, N.-J. Guo, L.-K. Xie, J.-Y. Liu, Y.-H. Ma, J.-S. Tang, C. Zhang, C.-F. Li, and G.-C. Guo, Direct non-Hermitian measurement and uncertainty relation for the high-dimensional quantum domain, Phys. Rev. Appl. **24**, 024006 (2025).
[62] C. Wang, Z. Fu, W. Mao, J. Qie, A. D. Stone, and L. Yang, Non-Hermitian optics and photonics: From classical to quantum, Adv. Opt. Photon. **15**, 442 (2023).
[63] J. Xu, Y. Mao, Z. Li, Y. Zuo, J. Zhang, B. Yang, W. Xu, N. Liu, Z. J. Deng, W. Chen, K. Xia, C.-W. Qiu, Z. Zhu, H. Jing, and K. Liu, Single-cavity loss-enabled nanometrology, Nat. Nanotechnol. **19**, 1472 (2024).
[64] Y.-P. Ruan, J.-S. Tang, Z. Li, H. Wu, W. Zhou, L. Xiao, J. Chen, S.-J. Ge, W. Hu, H. Zhang, C.-W. Qiu, W. Liu, H. Jing, Y.-Q. Lu, and K. Xia, Observation of loss-enhanced magneto-optical effect, Nat. Photonics **19**, 109 (2025).
[65] Y.-W. Lu, J.-F. Liu, R. Liu, R. Su, and X.-H. Wang, Quantum exceptional chamber induced by large nondipole effect of a quantum dot coupled to a nano-plasmonic resonator, Nanophotonics **10**, 2431 (2021).
[66] L. Xiao, Y. Chu, Q. Lin, H. Lin, W. Yi, J. Cai, and P. Xue, Non-Hermitian sensing in the absence of exceptional points, Phys. Rev. Lett. **133**, 180801 (2024).
[67] J. Zhang, E.-Z. Li, Y.-J. Wang, B. Liu, L.-H. Zhang, Z.-Y. Zhang, S.-Y. Shao, Q. Li, H.-C. Chen, Y. Ma, T.-Y. Han, Q.-F. Wang, J.-D. Nan, Y.-M. Yin, D.-Y. Zhu, G.-C. Guo, D.-S. Ding, and B.-S. Shi, Exceptional point and hysteresis trajectories in cold Rydberg atomic gases, Nat. Commun. **16**, 3511 (2025).
[68] Z. Dong, Z. Li, F. Yang, C.-W. Qiu, and J. S. Ho, Sensitive readout of implantable microsensors using a wireless system locked to an exceptional point, Nat. Electron. **2**, 335 (2019).
[69] Z.-P. Liu, J. Zhang, Ş. K. Özdemir, B. Peng, H. Jing, X.-Y. Lü, C.-W. Li, L. Yang, F. Nori, and Y.-X. Liu, Metrology with $\mathcal{PT}$-symmetric cavities: Enhanced sensitivity near the $\mathcal{PT}$-phase transition, Phys. Rev. Lett. **117**, 110802 (2016).
[70] A. Li, H. Wei, M. Cotrufo, W. Chen, S. Mann, X. Ni, B. Xu, J. Chen, J. Wang, S. Fan, C.-W. Qiu, A. Alù, and L. Chen, Exceptional points and non-Hermitian photonics at the nanoscale, Nat. Nanotechnol. **18**, 706 (2023).
[71] Z. Li, C. Li, Z. Xiong, G. Xu, Y. R. Wang, X. Tian, X. Yang, Z. Liu, Q. Zeng, R. Lin, Y. Li, J. K. W. Lee, J. S. Ho, and C.-W. Qiu, Stochastic exceptional points for noise-assisted sensing, Phys. Rev. Lett. **130**, 227201 (2023).
[72] Z. Xie, Y. Wang, Z. Li, and T. Li, Enhanced rotation sensing with high-order exceptional points in a multi-mode coupled-ring gyroscope, Opt. Lett. **49**, 3810 (2024).
[73] H. Wang, Y.-H. Lai, Z. Yuan, M.-G. Suh, and K. Vahala, Petermann-factor sensitivity limit near an exceptional point in a Brillouin ring laser gyroscope, Nat. Commun. **11**, 1610 (2020).
[74] H. Loughlin and V. Sudhir, Exceptional-point sensors offer no fundamental signal-to-noise ratio enhancement, Phys. Rev. Lett. **132**, 243601 (2024).
[75] W. Ding, X. Wang, and S. Chen, Fundamental sensitivity limits for Non-Hermitian quantum sensors, Phys. Rev. Lett. **131**, 160801 (2023).
[76] J. Wiersig, Prospects and fundamental limits in exceptional point-based sensing, Nat. Commun. **11**, 2454 (2020).
[77] H. Hodaei, A. U. Hassan, S. Wittek, H. Garcia-Gracia, R. El-Ganainy, D. N. Christodoulides, and M. Khajavikhan, Enhanced sensitivity at higher-order exceptional points, Nature (London) **548**, 187 (2017).
[78] Y.-H. Lai, Y.-K. Lu, M.-G. Suh, Z. Yuan, and K. Vahala, Observation of the exceptional-point-enhanced Sagnac effect, Nature (London) **576**, 65 (2019).
[79] W. Chen, Ş. K. Özdemir, G. Zhao, J. Wiersig, and L. Yang, Exceptional points enhance sensing in an optical microcavity, Nature (London) **548**, 192 (2017).
[80] Ş. K. Özdemir, S. Rotter, F. Nori, and L. Yang, Parity–time symmetry and exceptional points in photonics, Nat. Mater. **18**, 783 (2019).
[81] L. Chang, X. Jiang, S. Hua, C. Yang, J. Wen, L. Jiang, G. Li, G. Wang, and M. Xiao, Parity–time symmetry and variable optical isolation in active–passive-coupled microresonators, Nat. Photonics **8**, 524 (2014).
[82] M.-A. Miri and A. Alù, Exceptional points in optics and photonics, Science **363**, eaar7709 (2019).
[83] D. Leykam, K. Y. Bliokh, C. Huang, Y. Chong, and F. Nori, Edge modes, degeneracies, and topological numbers in non-Hermitian systems, Phys. Rev. Lett. **118**, 040401 (2017).
[84] T. Li, Z. Gao, and K. Xia, Nonlinear-dissipation-induced nonreciprocal exceptional points, Opt. Express **29**, 17613 (2021).
[85] W. Li, R. Liu, J. Li, J. Zhong, Y.-W. Lu, H. Chen, and X.-H. Wang, Highly efficient single-exciton strong coupling with plasmons by lowering critical interaction strength at an exceptional point, Phys. Rev. Lett. **130**, 143601 (2023).
[86] Y. Wu, W. Liu, J. Geng, X. Song, X. Ye, C.-K. Duan, X. Rong, and J. Du, Observation of parity-time symmetry breaking in a single-spin system, Science **364**, 878 (2019).
[87] C. Liang, C. Yang, W. Huang, and L. You, Exceptional point-enhanced Rydberg atomic electrometers, Phys. Rev. Lett. **136**, 053203 (2026).
[88] R. Kononchuk, J. Cai, F. Ellis, R. Thevamaran, and T. Kottos, Exceptional-point-based accelerometers with enhanced signal-to-noise ratio, Nature (London) **607**, 697 (2022).
[89] A. Metelmann and A. Clerk, Nonreciprocal photon transmission and amplification via reservoir engineering, Phys. Rev. X **5**, 021025 (2015).
[90] R. Belyansky, C. Weis, R. Hanai, P. B. Littlewood, and A. A. Clerk, Phase transitions in nonreciprocal driven-dissipative condensates, Phys. Rev. Lett. **135**, 123401 (2025).
[91] H. J. Kimble, Y. Levin, A. B. Matsko, K. S. Thorne, and S. P. Vyatchanin, Conversion of conventional gravitational-wave interferometers into quantum nondemolition interferometers by modifying their input and/or output optics, Phys. Rev. D **65**, 022002 (2001).
[92] P. Kok, W. J. Munro, K. Nemoto, T. C. Ralph, J. P. Dowling, and G. J. Milburn, Linear optical quantum computing with photonic qubits, Rev. Mod. Phys. **79**, 135 (2007).
[93] A. H. Safavi-Naeini, J. Chan, J. T. Hill, S. Gröblacher, H. Miao, Y. Chen, M. Aspelmeyer, and O. Painter, Laser noise in

cavity-optomechanical cooling and thermometry, New J. Phys. **15**, 035007 (2013).

[94] V. Giovannetti, S. Lloyd, and L. Maccone, Quantum-enhanced measurements: Beating the standard quantum limit, Science **306**, 1330 (2004).

[95] V. Giovannetti, S. Lloyd, and L. Maccone, Advances in quantum metrology, Nat. Photonics **5**, 222 (2011).

[96] K. Xia, N. Zhao, and J. Twamley, Detection of a weak magnetic field via cavity-enhanced Faraday rotation, Phys. Rev. A **92**, 043409 (2015).

[97] N. Zeng, T. Liu, K. Xia, Y.-R. Zhang, and F. Nori, Non-Hermitian sensing from the perspective of postselected measurements, Phys. Rev. Res. **7**, 043219 (2025).

[98] M. Zhang, W. Sweeney, C. W. Hsu, L. Yang, A. Stone, and L. Jiang, Quantum noise theory of exceptional point amplifying sensors, Phys. Rev. Lett. **123**, 180501 (2019).

[99] T. S. Karnik, X. Ren, C.-H. Lee, B.-H. Wu, M. Chaudhari, C. Cheung, J. Wang, S.-Y. Ma, M. J. Mehrabad, I. Christen, R. Kopparapu, K. Kwon, Y. Yu, S. K. Vadlamani, K. Kunes, Q. Zhuang, D. Englund, Z. Chen, and M. Yu, 18-dB on-chip vacuum squeezing in an adaptively poled lithium niobate waveguide, arXiv:2605.27607.

[100] C. Chen, L. Jin, and R.-B. Liu, Sensitivity of parameter estimation near the exceptional point of a non-Hermitian system, New J. Phys. **21**, 083002 (2019).